MNRAS **000**, 1–19 (2021) Preprint 7 December 2021 Compiled using MNRAS LATEX style file v3.0

High-mass pulsators in eclipsing binaries observed using TESS

John Southworth [1], Dominic M. Bowman [2]
[1] *Astrophysics Group, Keele University, Staffordshire, ST5 5BG, UK*
[2] *Institute of Astronomy, KU Leuven, Celestijnenlaan 200D, B-3001 Leuven, Belgium*

Accepted NNNN. Received NNNN; in original form NNNN.

ABSTRACT
Pulsating massive stars in eclipsing binary systems are important laboratories for constraining stellar structure and evolution theory. However, prior to the all-sky Transiting Exoplanet Survey Satellite (TESS) mission, few such systems had been discovered or studied in detail. We have inspected the TESS light curves of a large number of eclipsing binaries known to contain high-mass stars, and compiled a list of 18 objects which show intrinsic variability. The light curves were modelled both to determine the physical properties of the systems, and to remove the effects of binarity in order to leave residual light curves suitable for asteroseismic analysis. Precise mass and radius measurements were obtained for δ Cir, CC Cas, SZ Cam V436 Per and V539 Ara. We searched the residual light curves for pulsation signatures and found eleven objects to contain a definite or possible β Cephei star, six to contain slowly pulsating B (SPB) stars, and eight to to have residual light curves dominated by stochastic low-frequency (SLF) variability. The large number of pulsating eclipsing systems we have identified makes asteroseismology of high-mass stars in eclipsing binaries a feasible avenue to constrain the interior physics of a large sample of massive stars for the first time.

Key words: stars: fundamental parameters — stars: binaries: eclipsing — stars: oscillations

1 INTRODUCTION

High-mass stars are preferentially found in binary and multiple systems (Sana et al. 2012, 2014; Kobulnicky et al. 2014) and a significant fraction have short orbital periods. They are also bright so are over-represented in magnitude-limited samples. As a result, a relatively large number of high-mass stars have been found to be members of eclipsing binaries (EBs). Of particular interest are high-mass stars in EBs with orbital periods long enough for them to have evolved as single stars. For these objects it is possible to measure their masses and radii directly and use these properties to compare with or to calibrate theoretical models of stellar evolution of single stars (e.g. Andersen et al. 1990; Ribas et al. 2000; Torres et al. 2010). A prominent recent trend is the finding that the properties of high-mass EBs need stronger internal mixing processes than predicted by standard evolutionary models (Tkachenko et al. 2020; Johnston 2021). Subsequent evolution of high-mass short-period binaries leads to a wide variety of exotic objects that are important for many areas of stellar astrophysics, such as X-ray binaries, supernovae and gamma-ray bursts (Podsiadlowski et al. 2002, 2004; Belczynski et al. 2020; Chrimes et al. 2020).

Many high-mass stars also show pulsations (Bowman 2020). Among early-type main-sequence stars of spectral type types O and B, there are three main classes of pulsating variable. The slowly pulsating B (SPB) stars are mid-to-late B stars that pulsate in high-radial order gravity (g) modes with periods of order days (Waelkens 1991). The β Cephei stars span spectral types from O9 to B3 on the main sequence but can reach B5 during the giant phase. They pulsate in low-radial order pressure (p) and g modes with periods of order a few hours (Stankov & Handler 2005). The pulsation modes of SPB and β Cephei stars are driven by a heat-engine mechanism operating in the partial ionisation zones of iron and nickel at 200 000 K (Dziembowski & Pamyatnykh 1993; Dziembowski et al. 1993). This opacity-based driving mechanism produces periodic standing waves (i.e. coherent pulsation modes), from which forward asteroseismic modelling can reveal a star's interior physics (Aerts et al. 2010; Aerts 2021). See Bowman (2020) for a recent review of forward asteroseismic results of SPB and β Cephei stars. In particular, the combination of dynamical masses and radii from binary modelling with asteroseismic modelling of pulsations in eclipsing systems has shown great promise in being able to precisely constrain stellar structure and evolution theory (see e.g. Schmid & Aerts 2016; Johnston et al. 2019). But such studies are so far lacking among massive stars.

The third type of pulsator among early-type stars are those which exhibit stochastic low-frequency (SLF) variability (Bowman et al. 2019a,b, 2020). Such stars have quasi-periodic and time-dependent variability spanning a broad range of periods from several days to of order minutes, which has been inferred to be caused by stochastically excited gravity waves driven by turbulent (core) convection (Bowman et al. 2019b). These gravity waves are an efficient mixing mechanism inside massive stars (Rogers & McElwaine 2017), and are seemingly ubiquitous in massive stars with precise enough photometry (Bowman et al. 2019a). Gravity waves are excited at the interface of convective and radiative regions inside massive stars, which include

the convection core as predicted by two- and three-dimensional hydrodynamical simulations (Rogers et al. 2013; Edelmann et al. 2019; Horst et al. 2020). Another explanation for SLF variabilty in massive stars is caused by the dynamics of their turbulent envelopes, which also gives rise to temperature and velocity variations (Cantiello et al. 2021; Schultz et al. 2021). A comparison of recent high-cadence TESS photometry and high-resolution spectroscopy allowed Bowman et al. (2020) to demonstrate that the SLF variability in massive stars probex the mass and age of a star, and offer further support to the conclusion that gravity waves are responsible for macroturbulence in massive stars (Aerts et al. 2009; Simón-Díaz et al. 2010; Grassitelli et al. 2015, 2016; Simón-Díaz et al. 2017). Therefore the continued study of SLF variability, especially in binary systems that have so far been neglected, is an exciting prospect for constraining the interior mixing of massive stars as so far their study has been mainly based on single stars. To do so, a well-characterised sample of massive binary systems is needed, which is one of the motivations of this work.

In this work we present the discovery and preliminary analysis of a set of pulsating high-mass stars in EBs. A detailed study of these systems in most cases will require extensive spectroscopy and sophisticated analysis, which we leave to future work. We have also determined the physical properties of targets for which suitable data were available.

2 TARGET SELECTION

Only a few EBs containing high-mass pulsators were known until recently. The main reason for this is that the amount of data needed to securely detect pulsations photometrically is much higher compared to their single-star counterparts. Furthermore, disentangling the photometric signals of binarity, rotation and pulsations of massive stars require ultra-high photometric precision, which is difficult to achieve from the ground. SPB and β Cephei stars are observationally difficult to detect because of their low pulsation amplitudes (certainly compared to eclipse depths); SPB stars also have pulsation periods longer than a single night so are difficult to study using ground-based observations. We note that some high-mass pulsators in EBs have been identified spectroscopically (e.g. V2107 Cyg; Bakış et al. 2014) through line-profile variations (LPVs).

The *Kepler* space mission brought a huge improvement in the quality and quantity of time-series photometry for pulsating stars, but its small sky coverage meant few high-mass stars were observed and even fewer high-mass pulsators in EBs were identified. The prime example of this is the discovery of SLF variability in the B1.5 III + B2 V system V380 Cyg (Tkachenko et al. 2012, 2014). The appearance of TESS (Ricker et al. 2015) has changed this picture completely as it is in the process of obtaining time-series high-precision photometry of a large fraction of the sky. In contrast to *Kepler*, the TESS mission has observed a large number of high-mass EBs, of which many have an extensive observational history and in some cases a detailed characterisation of the physical properties of the component stars. See the recent study by IJspeert et al. (2021) for a census of EBs with g-mode pulsations predominantly focussed on intermediate-mass stars, Prša et al. (2021) for a catalogue of 4500 EBs detected using TESS, and Southworth (2021) for a detailed review of the impact of space-based telescopes on binary star science.

We therefore searched the TESS database to find EBs containing high-mass pulsating stars. The starting list was taken to be a bibliography of objects gradually accumulated by the first author since the year 2001, and therefore includes only those EBs identified as such in a past publication. Each one was entered in the data visualisation portal at the Mikulski Archive for Space Telescopes (MAST) archive[1] and any available short-cadence light curves were visually inspected for relevant features. This target selection was performed manually in summer 2020 – many more of these objects will be detectable using automated methods and subsequent TESS data.

The targets considered in this work are shown in Table 1. We have previously published the discovery and initial analysis of two EBs containing β Cephei stars: V453 Cyg (Southworth et al. 2020) and VV Ori (Southworth et al. 2021). Two other systems we found have since been the subject of an analysis by others: CW Cep (Lee & Hong 2021) and V Pup (Budding et al. 2021). We include these four systems in our list of targets but do not study them further.

Labadie-Bartz et al. (2020) recently presented the discovery of five new β Cephei EBs using photometry from the KELT project (Pepper et al. 2007). The TESS light curves of these objects confirm the nature in three cases (V447 Cep, HD 339003 and HD 344880). A fourth object, HD 227977, shows β Cephei pulsations but not eclipses in the TESS light curve so is unlikely to be a β Cephei EB. The fifth star, HD 254346, has no TESS light curve but was considered to be a probable blend rather than a β Cephei EB (Labadie-Bartz et al. 2020). We have not considered these objects further in the current work, as Labadie-Bartz et al. (2020) state they are already following them up.

3 OBSERVATIONS

TESS was launched by NASA on 2018/04/08 into an eccentric orbit around the Earth resonant with the orbit of the Moon (Ricker et al. 2015). It is currently performing a photometric survey of 85% of the celestial sphere with the aim of identifying extrasolar planets through the transit method (Ricker et al. 2015). The observational equipment comprises four cameras with 10.5 cm apertures, each with four CCDs, that together image a contiguous $24^\circ \times 96^\circ$ strip of sky. The pixel size on the sky is $21'' \times 21''$, so contamination occurs for many stars. TESS observes through a wide-band filter that covers approximately 600 nm to 1000 nm.

Each strip of sky is observed by TESS for two orbits (27.4 d), with a break near the midpoint for downlink of data to Earth. Each set of observations is called a sector, and some sky areas are observed in multiple sectors. A total of 200 000 stars were preselected for high-cadence observations (summed into a 120 s sampling rate on board the satellite). Full-frame images are also captured at a cadence of 1800 s (again summed on board), and subsequently clipped into an effective integration time of 1425 s by a cosmic-ray rejection algorithm.

The data are processed and released as light curves by the TESS Science Processing Operations Center (SPOC) for stars observed at high cadence (Jenkins et al. 2016). The standard data product is simple aperture photometry (SAP). An additional data product, pre-search data conditioning (PDC) light curves, is available which has been processed to make it more suitable for detecting shallow transits of extrasolar planets in front of their host stars.

[1] `https://mast.stsci.edu/portal/Mashup/Clients/Mast/Portal.html`

Table 1. Basic information for the targets considered in this work. For simplicity they are given in alphabetical order, beginning with numbers then Greek letters then Latin letters. The spectral types come from a variety of sources, with ones from refereed journal articles preferred.

Target	HD number	V magnitude	Spectral type	Orbital period (d)	Pulsation type	TESS sector(s)	Analysis of TESS data
16 Lac	216916	5.59	B2 IV	12.097	β Cephei	16	This work
δ Cir	135240	5.04	O7 III-V + O9.5 V + B0.5 V	3.902	SLF	12	This work
η Ori	35411	3.34	B1 V + B2:	7.988	β Cephei	6, 32	This work
λ Sco	158926	1.62	B1.5 IV + PMS + B2 V	5.953	β Cephei	12, 39	This work
μ Eri	30211	4.01	B5 IV	7.381	SLF + SPB?	5,32	This work
AN Dor	31407	7.69	B2/3 V	2.033	β Cephei	2–6, 29–32	This work
AR Cas	221253	4.89	B3 V	6.067	SPB	17, 24	Southworth et al. (in prep.)
AS Cam	35311	8.60	A0 V	3.431	SPB	19, 52	Southworth et al. (in prep.)
CC Cas	19820	7.10	O8.5 III + B0.5 V	3.366	SLF	18, 19	This work
EM Car	97484	8.51	O7.5 V((f)) + O7.5 V((f))	3.415	SLF	10, 11, 37	Torres et al. (in prep.)
EO Aur	34333	7.76	B0 V + B3 V	4.065	β Cephei	19	This work
CW Cep	218066	7.64	B1.5 Vn	2.729	β Cephei	17, 18, 24	Lee & Hong (2021)
FZ CMa	42942	8.09	B2 V + B2 V	1.273	β Cephei	7, 33	This work
HD 217919	217919	8.27	B0.5 III	16.206	β Cephei?	17, 18, 24	This work
HQ CMa	57593	5.99	B3 V	unknown	β Cep/SPB hybrid?	7, 34, 35	This work
LS CMa	52670	5.64	B2-3 III-IV	70.23	β Cephei? SPB?	6, 7, 33, 34	This work
QX Car	86118	6.64	B2 V	4.478	β Cephei?	9, 10, 36, 37	Torres et al. (in prep.)
SZ Cam	25638	6.93	O9 IV + B0.5 V	2.698	SLF	19	This work
V Pup	65818	4.47	B1 Vp + B2:	1.454	β Cephei	7, 9, 34, 35	Budding et al. (2021)
V379 Cep	197770	6.31	B2 IV-III	99.764	SLF	15–17	This work
V436 Per	11241	5.53	B1.5 V	25.936	SLF	18	This work
V446 Cep	210478	7.73	B1 V + B9 V	3.808	β Cephei + TEO?	16, 17, 24	This work
V453 Cyg	227696	8.40	B0.4 IV + B0.7 IV	3.890	β Cephei	14, 15, 41	Southworth et al. (2020)
V539 Ara	161783	5.68	B3 V + B4 V	3.169	SLF + SPB?	13, 39	This work
V2107 Cyg	191473	8.63	B1 III	4.284	β Cephei	14, 15, 41	This work
VV Ori	36695	5.34	B1 V + B7 V	1.495	β Cephei + SPB	6, 32	Southworth et al. (2021)

The PDC data are not intended for stars which show large variability amplitudes, such as many EBs, and in our experience often contain strong systematics introduced by the conditioning process. We therefore used the SAP data for every object in the current work. These were downloaded from the MAST, extracted from the fits files, and converted into magnitude units. We rejected any datapoints having a nonzero flag for the QUALITY parameter, with the exception of a few cases noted below. We also ignored the errorbars provided as these are usually far too small and the data are relatively homogeneous, preferring instead to determine the quality of our modelling from the scatter of the data around the best fits. Light curves for each of our targets are shown in Figs. 1, 2 and 3.

4 ANALYSIS METHODS

4.1 Analysis of eclipses

The first analysis step was to attempt to model the effects of binarity in the TESS light curve. This served dual aims: to measure the radii and orbital inclination of the component stars, and to subtract the signatures of binarity from the light curve prior to investigation of the pulsations. For this step we used version 42 of the JKTEBOP[2] code (Southworth et al. 2004; Southworth 2013). This code treats the stars as spheres for the calculation of eclipse shapes and as ellipsoids for the simulation of the ellipsoidal effect. Such an approximation is suitable for systems where the stars are not very tidally deformed, and in the case of well-detached systems JKTEBOP has been shown to agree very well with other codes (Maxted et al. 2020). For close binaries where the components are significantly aspherical, JKTEBOP still provides a good fit to the data but the parameters of the fit become unreliable. In some cases we have continued to use JKTEBOP in preference to more sophisticated codes because we find that it is orders of magnitude faster both for the user and the computer; we give the approximate parameters of the system for reference but leave detailed modelling to the future.

Throughout this paper we refer to the primary star (the one obscured at the deeper eclipse) as star A. The secondary star is star B and any tertiary star (if present) is called star C.

In JKTEBOP the radii of the stars are parameterised in terms of the fractional radii, defined by $r_{\rm A} = \frac{R_{\rm A}}{a}$ and $r_{\rm B} = \frac{R_{\rm B}}{a}$ where $R_{\rm A}$ and $R_{\rm B}$ are the true radii of the stars, and a is the semimajor axis of the relative orbit. The fitted parameters are the sum $(r_{\rm A} + r_{\rm B})$ and ratio $(k = \frac{r_{\rm B}}{r_{\rm A}})$ of the radii, as these are more closely related to the eclipse shapes. We also fitted for the orbital inclination (i), the ratio of the central surface brightnesses of the stars (J), the orbital period (P) and the time of midpoint of a primary eclipse (T_0). Limb darkening was included using the quadratic law (Kopal 1950) with theoretical coefficients for the TESS passband from Claret (2017); we typically fitted for the linear coefficients of the two stars ($u_{\rm A}$ and $u_{\rm B}$) and fixed the quadratic coefficients ($v_{\rm A}$ and $v_{\rm B}$) because of the strong correlations between u and v (Southworth et al. 2007b). In cases where the orbit was eccentric we additionally fitted the quantities $e\cos\omega$ and $e\sin\omega$, where e is the orbital eccentricity and ω is the argument of periastron. Some systems required the inclusion of third light (ℓ_3) as a fitted parameter. Finally, we fitted for the coefficients of low-order polynomials applied to the out-of-eclipse brightness of the systems as a function of time in order to

[2] http://www.astro.keele.ac.uk/jkt/codes/jktebop.html

remove any slow variations in brightness due to either astrophysical or instrumental effects.

4.1.1 *Wilson-Devinney code*

Some of the systems studied in this work have stars sufficiently close to each other to be significantly tidally distorted. In these cases a spherical-star approximation (as used in JKTEBOP) is not suitable and full Roche geometry is needed. Where the prospect of extracting useful information was large, we fitted the light curve with the Wilson-Devinney (WD) code (Wilson & Devinney 1971; Wilson 1979) in its 2004 version (WD2004), driven by the JKTWD wrapper (Southworth et al. 2011). Prior to this, we converted each light curve to orbital phase and then binned it into 400 datapoints in order to save computing time. These data were fitted in mode 0 or 2, assuming (pseudo)synchronous rotation, logarithmic limb darkening using coefficients from Van Hamme (1993), gravity darkening exponents of 1.0 as suitable for hot stars (Claret 1998) and albedos of 1.0. Mass ratios and effective temperature ($T_{\rm eff}$) values were taken from previous work and the Cousins R band was adopted as a reasonable approximation to the TESS passband for hot stars.

The fitted parameters in each case were the potentials of both stars, the orbital inclination, a phase shift, the light contributions of the two stars, the amount of third light in the system, and where necessary e and ω. Third light is expressed in terms of the fractional contribution to the total light of the system at a phase of 0.25, so is not directly comparable to the light contributions from the two stars individually (Wilson & Van Hamme 2004).

Error analysis with the WD code is non-trivial because the formal errors from the covariance matrix are usually too small, especially for data of space-based quality (Southworth 2020). We therefore perturbed the fit by changing the rotation rates, albedo and gravity darkening exponents by ±0.1, using a different limb darkening law, changing the mass ratio by its uncertainty, and trying different numerical resolutions (see Pavlovski et al. 2018 and Southworth 2020). The uncertainties were obtained from the variations between the different models and the final adopted parameter values and in all cases are larger than the formal errors calculated by WD2004.

4.2 Physical properties

Some objects have previously been studied spectroscopically, so their full physical properties can be calculated using the parameters measured from the light curve and published spectroscopic orbits. To do this we used the JKTABSDIM code (Southworth et al. 2005), which implements standard equations (e.g. Hilditch 2001) and propagates errorbars using a perturbation analysis. We used the IAU nominal solar properties and physical constants (Prša et al. 2016) for compatibility with other work. We calculated the masses of the stars ($M_{\rm A}$ and $M_{\rm B}$), their radii ($R_{\rm A}$ and $R_{\rm B}$), surface gravities ($\log g_{\rm A}$ and $\log g_{\rm B}$), light ratio in the TESS passband ($\ell_{\rm B}/\ell_{\rm A}$) and the semimajor axis (a).

Where possible we adopted published values for the $T_{\rm eff}$ values of the stars in order to calculate their luminosities ($L_{\rm A}$ and $L_{\rm B}$). Distances to the systems were not considered as this is beyond the scope of the current work. The results of this work are given in Tables 2, 3 and 4.

4.3 Pulsations

For the majority of systems, we used the residual light curve after subtracting the binary model to calculate an amplitude spectrum using a discrete Fourier Transform (Kurtz 1985). Similarly to Southworth et al. (2020, 2021), we identified significant pulsation frequencies and calculated their optimised parameters by non-linear least-squares fits to the residual light curve. We used a signal-to-noise ratio (S/N) $\geqslant 5$ as our significance criterion following previous studies of *Kepler* and TESS data that advocate using values larger than the canonical S/N $\geqslant 4$ limit of Breger et al. (1993) (see e.g. Burssens et al. 2020; Baran & Koen 2021; Bowman & Michielsen 2021). However, some stars had large pulsation amplitudes relative to their eclipse depths. This made binary modelling difficult without first identifying the dominant pulsation mode frequencies. Therefore for such stars we manually clipped the eclipses out of the light curve before performing frequency analysis. These systems were: 16 Lac, λ Sco and μ Eri.

It is common that in the case of an imperfect binary model, residual power is found at integer multiples of the orbital frequency (i.e. harmonics) in the amplitude spectrum of a residual light curve. If a significant frequency is extracted at the location of an orbital harmonic we do not consider it an independent pulsation frequency. This is because our goal is to identify stars with coherent heat-driven pulsations for future asteroseismic modelling. However, it is certainly plausible that at least some of the significant frequencies that coincide with orbital harmonics are tidally-excited oscillation (TEO) modes if the binary system is sufficiently eccentric (see e.g. Welsh et al. 2011; Thompson et al. 2012). However, differentiating TEO modes from residual amplitude from an imperfect binary model is beyond the scope of this work, as this requires more extensive spectroscopic monitoring and modelling. We are currently gathering spectroscopy of the most promising systems but leave the analysis for future work.

For each pulsation analysis, we produced a summary figure in the supplementary material, in which the top panel shows the residual light curve (i.e. after subtraction of the binary model) and the bottom panel shows the amplitude spectrum of the residual light curve with labelled significant pulsation mode frequencies. In the systems that had their eclipses removed prior to their frequency analysis, the significant frequencies are labelled in purple and are shown in Fig. A1. The summaries of other stars are shown in Figs. A2 and A3, and have their significant independent frequencies labelled in green. For each star, we also provide the pulsation mode frequencies, amplitudes and phases with uncertainties from the non-linear least-squares fit in Table A1. In Table 1 we also provide a pulsator classification for each target based on visual inspection.

5 DISCUSSION OF INDIVIDUAL OBJECTS

5.1 16 Lacertae = EN Lacertae

16 Lac is a very bright early-B-type EB showing shallow eclipses and gorgeous β Cephei pulsations. It was discovered to be a spectroscopic binary by Lee (1910), to be pulsating by Walker (1951), and to be eclipsing by Jerzykiewicz (1980). Star B has not been detected either photometrically or spectroscopically. Spectroscopic observations have been used to investigate the pulsations and to determine the spectroscopic orbit of the primary component (Lehmann et al. 2001; Aerts et al. 2003). Extensive photometry was obtained by Jerzykiewicz et al. (2015), who performed

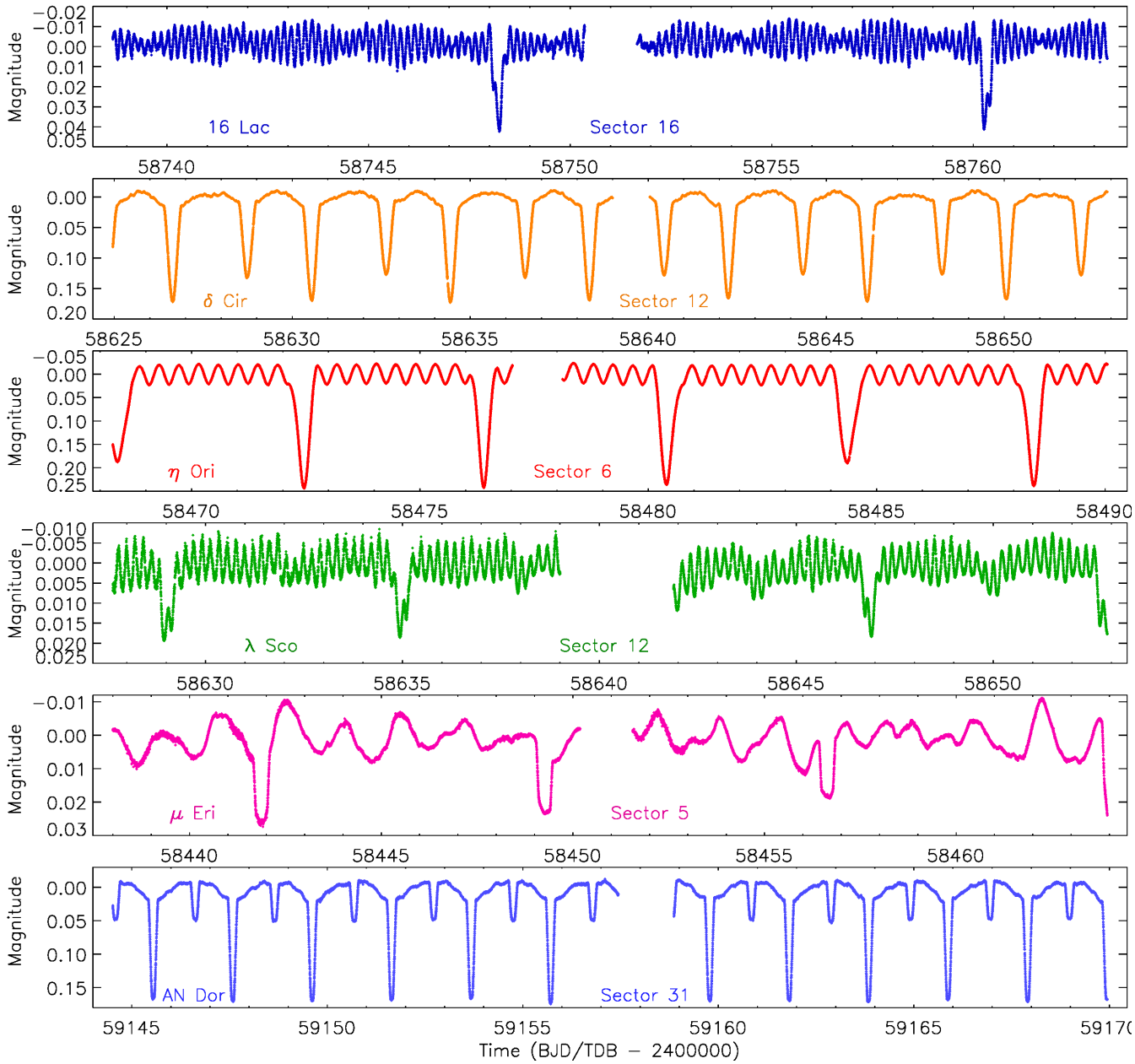

Figure 1. TESS light curves of the first six objects analysed in this work. In each case one sector is plotted. The object names and the sectors are labelled on the diagram.

a frequency analysis and a fit to the eclipses. Jerzykiewicz et al. (2015) found multiple frequencies attributable to β Cephei pulsations. 16 Lac has since been observed by TESS in Sector 16, but is not scheduled to be observed again by this satellite.

The TESS data from Sector 16 show clear multi-periodic pulsations with a maximum amplitude of approximately 0.01 mag, plus two consecutive eclipses of depth 0.04 mag (Fig. 1). We had to remove the requirement of QUALITY = 0 in order to avoid losing datapoints in the second half of the first eclipse; the flagged data appear to be as reliable as the data with QUALITY = 0. The eclipses are grazing and strongly distorted by the pulsations, so we elected to remove the pulsations before fitting the eclipses.

The secondary eclipse is shallow and smaller than the pulsations. It was not detected by Jerzykiewicz et al. (2015), who attributed this to it being very shallow due to the low $T_{\rm eff}$ of star B. After removal of the pulsations the secondary eclipse is identifiable at the correct orbital phase (0.511 based on the e and ω from Lehmann et al. 2001), representing the first direct detection of light from star B and confirming the interpretation of Jerzykiewicz et al. (2015). We removed the pulsations in two different ways and modelled both light curves with JKTEBOP, finding good consistency between the parameters. The orbital shape parameters (e and ω) were fixed at the values for the spectroscopic orbit of star A from Lehmann et al. (2001). Agreement is good for all parameters except J, for which we find 0.133 and 0.230 for the two light curves. Adopting $J = 0.18 \pm 0.05$ and $T_{\rm eff,1} = 22\,500$ K gives $T_{\rm eff,2} = 14700 \pm 1200$ K. The current TESS data (Fig. 1) are not definitive but do at least provide the first detection of the secondary

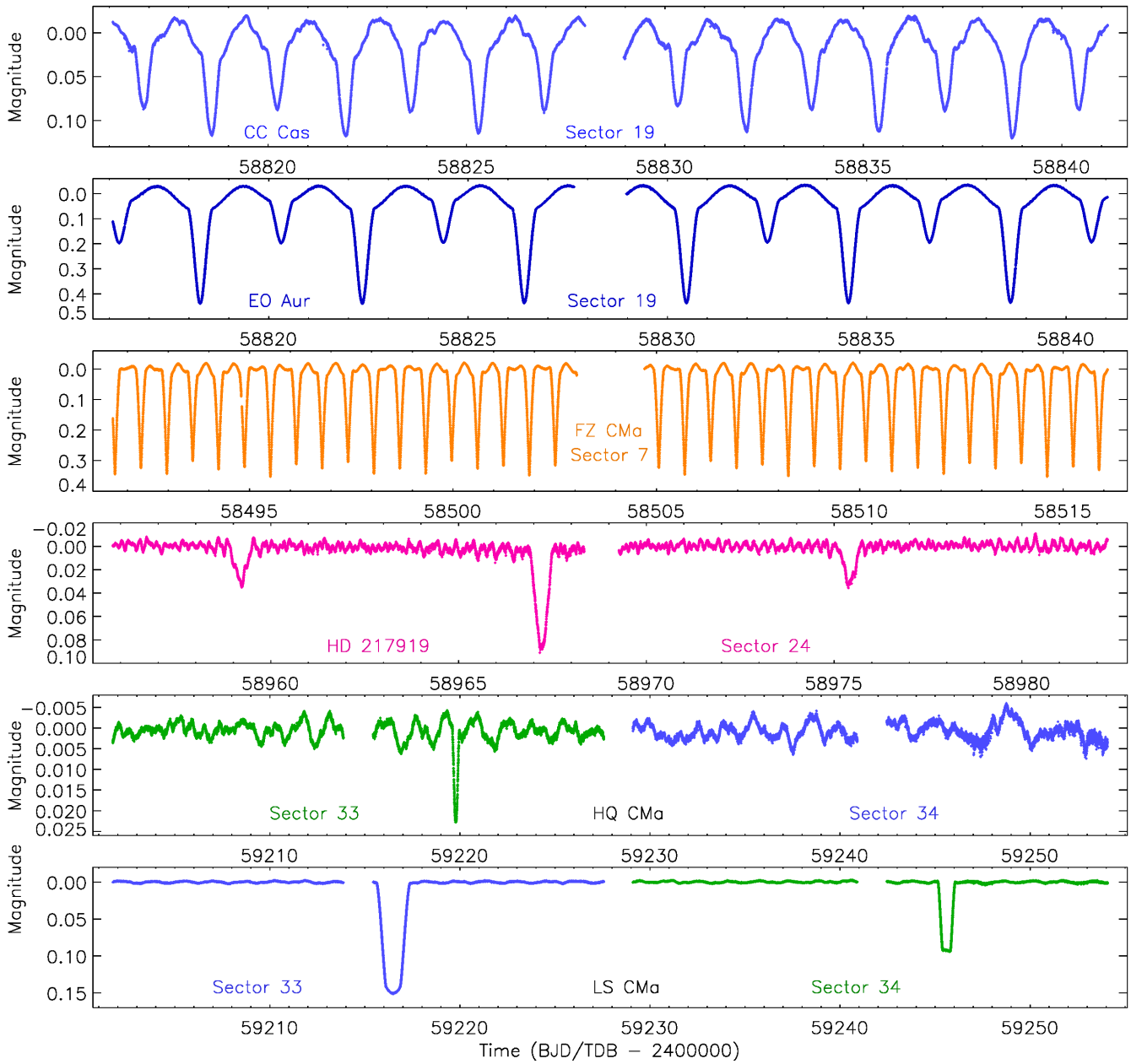

Figure 2. TESS light curves of the middle six objects analysed in this work. In four cases one sector is plotted, and in two cases two sectors are plotted. The object names and the sectors are labelled on the diagram.

eclipse. From the $r_{\rm B}$, i, $K_{\rm A}$ and P in Table 2 we can determine the surface gravity of star B (see Southworth et al. 2007a). We find $\log g_{\rm B} = 3.50 \pm 0.04$ which is lower than that of the primary. One explanation for this would be if star B is still in the pre-main-sequence evolutionary phase.

Owing to the large pulsation amplitude amplitudes of 16 Lac relative to the eclipse depths, the eclipse profiles are significantly affected by the pulsations which limits our binary modelling. We manually removed the primary eclipses from the TESS light curve of 16 Lac prior to our pulsation frequency analysis. The summary figure of 16 Lac is shown in Fig. A1, including its pre- and post-clipped light curve and labelled amplitude spectrum. Star A is known to be a multi-periodic β Cephei star, and our analysis of TESS data reveals a dominant pulsation mode frequency of 5.9105 ± 0.0001 d^{-1} with an amplitude of 5.65 ± 0.03 mmag. We detected a total of eight significant independent pulsation mode frequencies which span the frequency range of $1.5 < \nu < 11.5$ d^{-1}, which is a typical range for such stars.

5.2 δ Circinus

δ Cir is an O-type eclipsing binary that shows SLF variability in its TESS light curve similar to other O-type stars (Bowman et al. 2020). No intrinsic variability in either star has been previously reported, likely due to the difficulty of obtaining high-quality photometry of such a bright star. It has a small eccentricity, apsidal motion, and a third component on a wider orbit. Penny et al. (2001) discovered the third star in IUE spectra (see also Stickland et al.

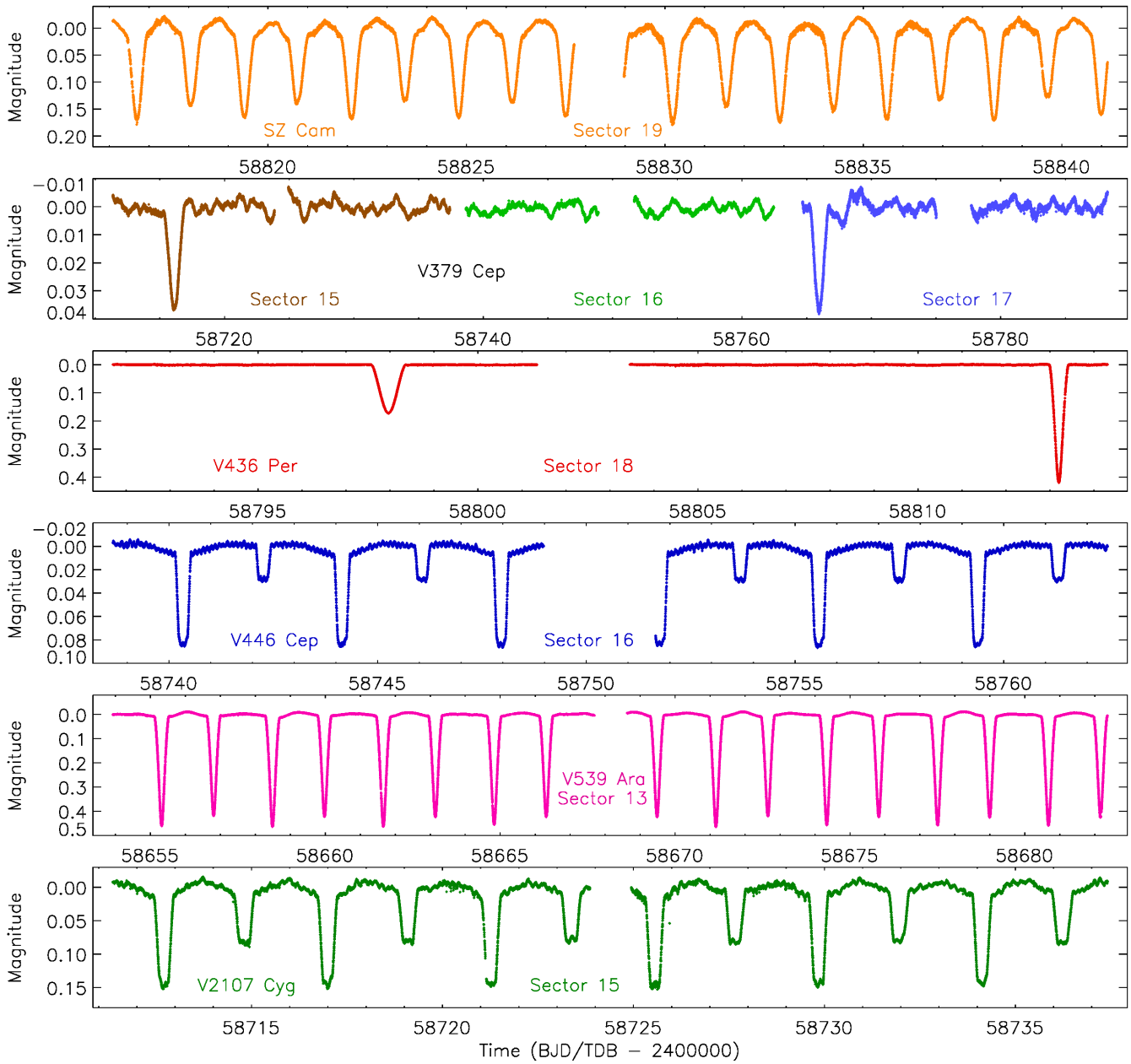

Figure 3. TESS light curves of the last six objects analysed in this work. In most cases one sector is plotted. The object names and the sectors are labelled on the diagram.

1993) and inferred spectral types of O7 III-V, O9.5 V and B0.5 V for the three components. Their preferred $T_{\rm eff}$ values were 37500 ± 1500 K, 33000 ± 1000 K and 29000 ± 2000 K, respectively. The most recent study was by Mayer et al. (2014), in which references to earlier work can be found. Mayer et al. favoured a spectral type of O8 IV for star A. They also interferometrically resolved star C using the VLTI, finding a magnitude difference of $\Delta H = 1.75$ mag (no uncertainty quoted) which corresponds to a fractional contribution of approximately 17% in the H-band.

δ Cir was observed by TESS in Sector 12 and the light curve shows eclipses of depth 0.17 mag (primary) and 0.13 mag (secondary) onto which a much lower-amplitude variability is superimposed (Fig. 1). Our fits require an orbital eccentricity that is small but highly significant and in good agreement with previous studies of this system.

Star A has a large fractional radius so we produced a preliminary fit of the light curve with JKTEBOP, phase-folded it, and performed a detailed analysis with WD2004 (Table 4 and Fig. 4). Due to the presence of a known third component we included ℓ_3 as a fitted parameter, obtaining a value of 0.277 ± 0.023. This is much larger than the 0.17 expected from the interferometrically-determined H-band magnitude difference, suggesting the presence of a fourth component, contaminating light in the large TESS aperture, or imperfect subtraction of background light during the data reduction process. Mayer et al. 2014 noted that some of the observed spectral line profiles were better fitted by four components, although its hierarchical position within the system is unclear,

Table 2. Physical properties of those systems for which a detailed analysis with JKTEBOP was possible. All times are given as BJD(TDB) − 2400000.

	16 Lac	η Ori	LS CMa	V436 Per	V446 Cep	V539 Ara
Fitted parameters:						
$r_A + r_B$	0.193 ± 0.003	0.2413 ± 0.0042	0.05779 ± 0.00019	0.08015 ± 0.00028	0.31624 ± 0.00067	0.3958 ± 0.0013
k	0.52 ± 0.02	0.7395 ± 0.0022	0.36559 ± 0.00070	1.097 ± 0.022	0.25676 ± 0.00042	0.786 ± 0.009
i (°)	80.2 ± 0.2	87.62 ± 0.42	89.461 ± 0.019	87.951 ± 0.025	85.58 ± 0.11	85.16 ± 0.13
J	0.18 ± 0.05	0.9044 ± 0.0042	0.6747 ± 0.0056	1.041 ± 0.022	0.4832 ± 0.0040	0.9601 ± 0.0035
ℓ_3	0.0 fixed	0.468 ± 0.016	0.0 fixed	-0.003 ± 0.011	0.0 fixed	0.0328 ± 0.0028
u_A	0.07 fixed	0.00 fixed	0.402 ± 0.081	0.046 ± 0.021	0.0910 ± 0.015	0.146 ± 0.023
u_B	0.10 fixed	0.00 fixed	0.10 fixed	$= u_A$	0.24 fixed	$= u_A$
v_A	0.22 fixed	0.35 fixed	-0.34 ± 0.14	0.22 fixed	0.08 fixed	0.21 fixed
v_B	0.22 fixed	0.35 fixed	0.22 fixed	0.22 fixed	0.24 fixed	0.21 fixed
$e \cos \omega$	0.017 fixed [a]	−0.00913±0.00010	−0.12541±0.00013	−0.12838±0.00011	0.00766±0.00011	−0.04600±0.00097
$e \sin \omega$	0.032 fixed [a]	0.0027±0.0033	−0.3281±0.0021	0.3614±0.0020	−0.0119±0.0019	−0.0311±0.0019
P (d)	12.095±0.002	7.98763±0.00032	70.02358±0.00034	25.935953±0.000034	3.808385±0.000004	3.169090±0.000021
T_0	58748.220±0.002	58480.4275±0.0003	59216.4877±0.0015	58813.2011±0.0001	58767.0005±0.0001	58671.1670±0.0003
K_A (km s^{-1})	23.818 ± 0.033 [a]	145.5 ± 0.03 [c]		97.4 ± 0.2 [d]	26600 ± 1000 [e]	150.4 ± 0.8 [f]
K_B (km s^{-1})		150 ± 3 [c]		91.2 ± 0.2 [d]	22200 ± 1000	176.6 ± 0.8 [f]
Derived parameters:						
r_A	0.1272 ± 0.0005	0.13871 ± 0.00066	0.04232 ± 0.00015	0.03822 ± 0.00051	0.25163 ± 0.00050	0.22171 ± 0.00055
r_B	0.0676 ± 0.0030	0.1026 ± 0.0019	0.01547 ± 0.00005	0.04191 ± 0.00029	0.06461 ± 0.00020	0.1742 ± 0.0016
e	0.0392 [a]	0.0095 ± 0.0010	0.3512 ± 0.0020	0.3835 ± 0.0018	0.0141 ± 0.0016	0.0555 ± 0.0011
ω (°)	63.7 [a]	164 ± 18	249.08 ± 0.14	109.56 ± 0.11	302.8 ± 4.3	214.2 ± 1.1
Light ratio	0.05 ± 0.02	0.496 ± 0.022	0.09094 ± 0.00025	1.253 ± 0.032	0.03186 ± 0.00026	0.5912 ± 0.0057
M_A ($\mathcal{M}_\odot^N$)		10.87 ± 0.44		6.880 ± 0.037		6.239 ± 0.066
M_B ($\mathcal{M}_\odot^N$)		10.54 ± 0.22		7.348 ± 0.039		5.313 ± 0.060
R_A ($\mathcal{R}_\odot^N$)		6.477 ± 0.073		3.415 ± 0.046		4.551 ± 0.019
R_B ($\mathcal{R}_\odot^N$)		4.79 ± 0.10		3.745 ± 0.027		3.575 ± 0.035
$\log g_A$ (c.g.s.)	3.95 ± 0.05 [b]	3.851 ± 0.010		4.209 ± 0.012		3.9170 ± 0.0029
$\log g_B$ (c.g.s.)	3.50 ± 0.04	4.100 ± 0.016		4.157 ± 0.006		4.0570 ± 0.0084
$T_{\rm eff,A}$ (K)	23200 ± 200 [b]	26600 [c]		21500 ± 1000 [d]		18100 ± 500 [g]
$T_{\rm eff,B}$ (K)	14700 ± 1200	25950		22000 ± 1000 [d]		17100 ± 500 [g]
$\log(L_A/\mathcal{L}_\odot^N)$				3.351 ± 0.081		3.302 ± 0.048
$\log(L_B/\mathcal{L}_\odot^N)$				3.471 ± 0.079		2.993 ± 0.052

References: [a] Lehmann et al. (2001); [b] Nieva & Przybilla (2012); [c] De Mey et al. (1996); [d] Taken from Janík et al. (2003). The errorbars for K_A and K_B have been doubled. No errorbars were given for the $T_{\rm eff}$ values so errorbars of 1000 K have been assumed.
[e] Çakırlı et al. (2014); [f] Andersen (1983); [g] Clausen (1996);

which supports the larger third light value we find. Future analyses would benefit from additional constraints on ℓ_3 in the TESS passband, perhaps through further optical or near-IR interferometry.

We determined the physical properties of the system from the results of our WD analysis and the velocity amplitudes from Penny et al. (2001). The velocity amplitude of star B found by Mayer et al. (2014) is significantly larger, but was not supplied with an errorbar so we were do not use it. We find masses in good agreement with those from Penny et al. (2001) but not Mayer et al. (2014), and radii in good agreement with those from Mayer et al. (2014). Although the mass measurements have precisions of 2–3% their true uncertainty is larger than this; the radius measurements should be reliable.

We detected no significant independent pulsation modes in the residual amplitude spectrum of δ Cir, as shown in Fig. A2. The light curve is dominated by SLF variability, which is typical for stars of spectral type of mid-to-late O. Furthermore, we note that since the system contains more than a single O-type star, the light curve (and amplitude spectrum) dominated by SLF variability has contributions for stars of different mass and age. Hence the flux dilution of each star's variability based on their relative light contributions is an important factor when interpreting SLF variability in multiple systems.

5.3 η Orionis

η Ori is a system of at least five early-type stars showing multiple types of photometric variability. Components A and B form a visual double separated by 1.8″, and component C is distant by 114″ (Balega et al. 1999; Mason et al. 2001). Component A is itself a spectroscopic triple system comprising an EB (Kunz & Stebbins 1916) with a period of 7.99 d (η Ori Aa,b) orbited by a tertiary with a 9 yr period (η Ori Ac). A photometric variability with a period of 0.301 d has been found to occur in the AB system, possibly arising from star Ab (Koch et al. 1980; Beardsley & Zizka 1980). This periodicity was corrected to 0.432 d by Waelkens & Lampens (1988). De Mey et al. (1996) obtained spectroscopic observations and detected LPVs with a period of 0.13 d that could be ascribed to a non-radial pulsation mode of angular degree $\ell = 4$ and azimuthal order $m = -3$. The Aa,b and Ac system has also been spatially resolved using lucky spectroscopy (Maíz Apellániz et al. 2018). These authors found spectral types of B0.7 V for Aa and B1.5 V for B, but were unable to identify Ab in their spectrum. Maíz Apellániz et al. (2018) also found that component B consists of two stars with high rotational velocities and a large radial velocity (RV) separation. This is consistent with the idea suggested by Lee et al. (1993) that component B is a 0.864 d contact binary and

Table 3. Physical properties of those systems for which an approximate analysis with JKTEBOP was performed. Quantities in brackets are uncertainties in the final digits of the preceding numbers. All times are given as BJD(TDB) − 2400000.

	λ Sco	μ Eri	AN Dor	EO Aur	HD 217919	V379 Cep	V2107 Cyg
Fitted parameters:							
$r_A + r_B$	0.32	0.40	0.40	0.44	0.17	0.072	0.38
k	0.17	0.28	0.35	0.62	0.41	0.96	0.34
i (°)	80.0	68.4	80.8	83.1	83.2	86.9	86.1
J	0.26	0.15 fixed	0.051	0.76	0.80	0.96	0.59
ℓ_3	0.54 fixed	0.0 fixed	0.0 fixed	0.0 fixed	0.20	0.50 fixed	0.0 fixed
u_A	0.05 fixed	0.10 fixed	0.33	0.05 fixed	0.05 fixed	0.07 fixed	0.05
u_B	0.24 fixed	0.18 fixed	0.24 fixed	0.25 fixed	0.28 fixed	0.07 fixed	0.10 fixed
v_A	0.15 fixed	0.22 fixed	0.10 fixed	0.09 fixed	0.07 fixed	0.22 fixed	0.22 fixed
v_B	0.25 fixed	0.29 fixed	0.21 fixed	0.21 fixed	0.20 fixed	0.22 fixed	0.21 fixed
$e \cos \omega$	0.033		0.043	0.0 fixed	0.009	0.0 fixed	−0.015
$e \sin \omega$	−0.032		−0.033	0.0 fixed	0.124	0.0 fixed	0.030
P (d)	5.94501	7.3813 (3)	2.032671 (1)	4.065556 (3)	16.20566 (5)	99.7638 fixed	4.284446 (15)
T_0 (BJD/TDB)	58634.974	58449.2324 (3)	59155.71301 (1)	58830.47762 (5)	58805.1534 (3)	58716.1004 (8)	58712.70759 (6)
K_A (km s^{-1})	39.3 ± 0.4 [a]	24.24 ± 0.53 [b]				43.4 [c]	104 [d]
K_B (km s^{-1})						79.7 [c]	187 [d]
Derived parameters:							
r_A	0.28	0.31	0.30	0.27	0.12	0.037	0.29
r_B	0.046	0.09	0.10	0.17	0.05	0.035	0.097
e	0.047	0.344 fixed [b]	0.054	0.0	0.124	0.0	0.034
ω (°)	315	160.5 fixed [b]	322		85.8		117
Light ratio	0.0072	0.01	0.0067	0.29	0.13	0.87	0.066
M_A ($\mathcal{M}_\odot^N$)						12.5	7.1
M_B ($\mathcal{M}_\odot^N$)						6.8	3.9
R_A ($\mathcal{R}_\odot^N$)						8.9	7.1
R_B ($\mathcal{R}_\odot^N$)						8.5	2.4
log g_A (c.g.s.)		3.55 ± 0.04 [b]				3.6	3.6
log g_B (c.g.s.)	4.44					3.4	4.3
$T_{eff,A}$ (K)	25000 ± 1000 [a]	15590 ± 120 [b]				22000 [c]	22500 ± 1500 [d]
$T_{eff,B}$ (K)						20200 [c]	15200 ± 1600 [d]
$\log(L_A/\mathcal{L}_\odot^N)$							4.1
$\log(L_B/\mathcal{L}_\odot^N)$							2.4

References: [a] Uytterhoeven et al. (2004a); [b] Jerzykiewicz et al. (2013); [c] Harmanec et al. (2007); [d] Bakış et al. (2014).

the shorter-period variation is actually due to the effects of binarity in this object.

η Ori was observed by TESS in sectors 6 and 32 (Fig. 1), and is not scheduled to be observed again. Both light curves show eclipses with a period of 7.988 d and a sinusoidal variability with a 0.43 d period. The features in the data from sector 32 have a much lower amplitude, implying difficulties in extracting reliable light curves for a star this bright, so we restricted our analysis of the data from sector 6. Here the eclipses are of depth 0.23 and 0.21 mag, and the sinusoidal variability has a period of 0.43207 d and an amplitude of 0.021 mag.

Our initial fits to the eclipses in the TESS data showed large residuals due to the shorter-period variation, so we proceeded with fits including a sine term to account for it. This yields a much better result (Table 2), but a more detailed analysis is needed for this object. The ratio of the variability periods is 18.4869 ± 0.0001, which is not consistent with any orbital commensurabilities. The shorter-period variability appears to be strictly periodic and also not exactly sinusoidal in shape, consistent with the ellipsoidal effect arising from a close binary. We conclude that the available data are plausibly explain as arising from a quintuple star system containing two binary systems: a detached EB with a period of 7.988 d and one component showing g-mode pulsations, and a non-eclipsing binary with a period of 0.8641 d and strong ellipsoidal variations.

5.4 λ Scorpii

λ Sco is a very bright system that has been studied extensively in the past. The inner binary is eclipsing and is composed of a B-star ($10.4 \pm 1.3\,M_\odot$) showing β Cephei pulsations and a 1.6–2.0 $M_\odot$ unevolved MS star; it has an orbital period of 5.953 d and eccentricity of 0.26. The tertiary component is a B-star ($8.1 \pm 1.0\,M_\odot$) on a much wider orbit of period 2.96 yr that has been interferometrically resolved. Extensive information and analysis of this system can be found in De Mey et al. (1997), Uytterhoeven et al. (2004a,b) and Tango et al. (2006), and a more recent study can be found in Handler & Schwarzenberg-Czerny (2013).

λ Sco was observed by TESS in Sectors 12 (Fig. 1) and 39, but only the first was available at the time of our analysis. We accepted all measurements with finite SAP flux values, irrespective of their QUALITY flag, giving 16 088 brightness measurements. The TESS light curve exhibits shallow eclipses and strong β Cephei variability. However, the eclipse depths (0.015 and 0.005 mag) are in poor agreement with those in an unpublished light curve (0.04 and 0.01 mag) from the WIRE satellite (Bruntt & Southworth 2008) so these data may not be reliable.

We nevertheless proceeded to fit the TESS data with JKTEBOP (Table 3). We fixed the third light at 0.54 based on the interferometric measurement at 700 nm from Tango et al. (2006). Our solution has a much lower eccentricity than in previous studies,

Table 4. Physical properties of those systems for which an analysis with JKTWD was performed. All times are given as BJD(TDB) − 2400000.

	δ Cir	CC Cas	FZ CMa	SZ Cam
Parameters from JKTEBOP*:*				
P (d)	3.902493 ± 0.000025	3.366029 ± 0.000024	1.273071 ± 0.000008	2.69863 ± 0.0003
T_0 (BJD/TDB)	58638.34812 ± 0.00009	58811.83691 ± 0.00013	58501.87752 ± 0.00003	58827.49911 ± 0.00009
WD control and fixed parameters:				
WD mode	2	0	2	2
Treatment of reflection	1	1	1	1
Number of reflections	1	1	1	1
Limb darkening law	logarithmic	logarithmic	logarithmic	logarithmic
Numerical grid size (normal)	40	40	60	60
Numerical grid size (coarse)	30	30	50	60
$T_{\rm eff}$ of star A (K)	37500	34500 [b]	22000 [d]	30320 ± 150 [e]
$T_{\rm eff}$ of star B (K)	n/a	29000 [b]	n/a	28015 ± 130 [e]
Rotation rate for star A	1.0	1.0	1.0	1.0
Rotation rate for star B	1.0	1.0	1.0	1.0
Albedo for star A	1.0	1.0	1.0	1.0
Albedo for star B	1.0	1.0	1.0	1.0
Gravity darkening exponent for star A	1.0	1.0	1.0	1.0
Gravity darkening exponent for star B	1.0	1.0	1.0	1.0
Logarithmic LD coefficient star A	0.2353	0.2465	0.2070	0.2597
Logarithmic LD coefficient star B	0.2097	0.2124	0.2032	0.2374
WD fitted parameters:				
Potential of star A	4.204 ± 0.029	3.284 ± 0.038	4.55 ± 0.07	3.43 ± 0.22
Potential of star B	4.815 ± 0.067	3.181 ± 0.057	4.57 ± 0.20	4.22 ± 0.48
Orbital inclination (°)	77.80 ± 0.19	65.44 ± 0.21	88.05 ± 0.20	83.0 ± 1.9
Orbital eccentricity	0.05868 ± 0.0048	0.0099 ± 0.0013	0.0	0.0
Argument of periastron (°)	353.6 ± 4.3	209 ± 27	n/a	n/a
Light from star A	7.35 ± 0.28	9.67 ± 0.36	3.511 ± 0.084	4.75 ± 0.59
Light from star B	n/a	2.48 ± 0.14	n/a	n/a
$T_{\rm eff}$ of star B (K)	30400 ± 400	n/a	20241 ± 125	29910 ± 430
Linear LD coefficient star A	0.3794 (fixed)	0.52 ± 0.14	0.000 ± 0.086	0.457 ± 0.033
Linear LD coefficient star B	0.3561 (fixed)	0.42 ± 0.24	0.037 ± 0.084	0.445 ± 0.072
Third light	0.277 ± 0.023		0.4667 ± 0.0061	0.531 ± 0.046
$K_{\rm A}$ (km s^{-1})	153.0 ± 1.4 [a]	123.9 ± 2.0 [c]	215 ± 8 [d]	185.2 ± 2.8 [e]
$K_{\rm B}$ (km s^{-1})	268.2 ± 2.8 [a]	292.4 ± 4.6 [c]	217 ± 11 [d]	247.0 ± 3.6 [e]
Derived parameters:				
$r_{\rm A}$	0.2812 ± 0.0018	0.3570 ± 0.0043	0.2857 ± 0.0005	0.3706 ± 0.0093
$r_{\rm B}$	0.1618 ± 0.0025	0.2245 ± 0.0055	0.2822 ± 0.0026	0.2087 ± 0.0092
$M_{\rm A}$ ($\mathcal{M}_\odot^{\rm N}$)	20.00 ± 0.50	23.49 ± 0.92	5.16 ± 0.56	13.22 ± 0.47
$M_{\rm B}$ ($\mathcal{M}_\odot^{\rm N}$)	11.41 ± 0.24	9.95 ± 0.34	5.11 ± 0.46	9.91 ± 0.35
$R_{\rm A}$ ($\mathcal{R}_\odot^{\rm N}$)	9.256 ± 0.091	10.87 ± 0.18	3.001 ± 0.094	8.61 ± 0.24
$R_{\rm B}$ ($\mathcal{R}_\odot^{\rm N}$)	5.326 ± 0.091	6.84 ± 0.18	2.964 ± 0.097	4.85 ± 0.22
$\log g_{\rm A}$ (c.g.s.)	$3.806 \pm 0,997$	3.736 ± 0.013	4.196 ± 0.022	3.689 ± 0.023
$\log g_{\rm B}$ (c.g.s.)	4.043 ± 0.014	3.766 ± 0.022	4.203 ± 0.018	4.063 ± 0.039
$\log(L_{\rm A}/\mathcal{L}_\odot^{\rm N})$	5.184 ± 0.070	5.179 ± 0.053	3.28 ± 0.16	4.752 ± 0.025
$\log(L_{\rm B}/\mathcal{L}_\odot^{\rm N})$	4.339 ± 0.090	4.474 ± 0.064	3.12 ± 0.19	4.116 ± 0.040

References: [a] Penny et al. (2001); [b] Hill et al. (1994); [c] Gorda (2013); [d] Moffat et al. (1983); [e] Tamajo et al. (2012).

and we recommend that a detailed analysis using more extensive data is performed when possible. The results are given in Table 2 to only a small number of significant figures. With the $K_{\rm A}$ from Uytterhoeven et al. (2004a) we were able to calculate the surface gravity of star B to be 4.44 (log cgs), which is appropriate for a low-mass MS star. This conclusively rules out the possibility that star B is a white dwarf (Berghöfer et al. 2000) and also disfavours the idea that it is a pre-MS star (Uytterhoeven et al. 2004a).

Similar to 16 Lac, λ Sco is a system for which the eclipse profiles are significantly affected by the pulsations which limits our binary modelling. We manually removed the eclipses from the TESS light curve prior to our frequency analysis, with its summary figure shown in Fig. A1. The primary of λ Sco is a known multi-periodic β Cephei star, and our analysis of the clipped TESS light curve reveals a dominant pulsation mode frequency of 4.6790 ± 0.0001 d^{-1} and amplitude of 4.02 ± 0.02 mmag, which is consistent in frequency to that detected by Uytterhoeven et al. (2004b) using spectroscopy. We detected a total of five significant independent pulsation mode frequencies which span the frequency range of $4 < \nu < 10$ d^{-1}. λ Sco was also recently identified as a candidate high-priority target for the upcoming ESA/KU Leuven CubeSpec space mission, which will assemble high-cadence and high resolution optical spectroscopy of massive stars, because of its high amplitude β Cephei pulsations (Bowman et al. 2021).

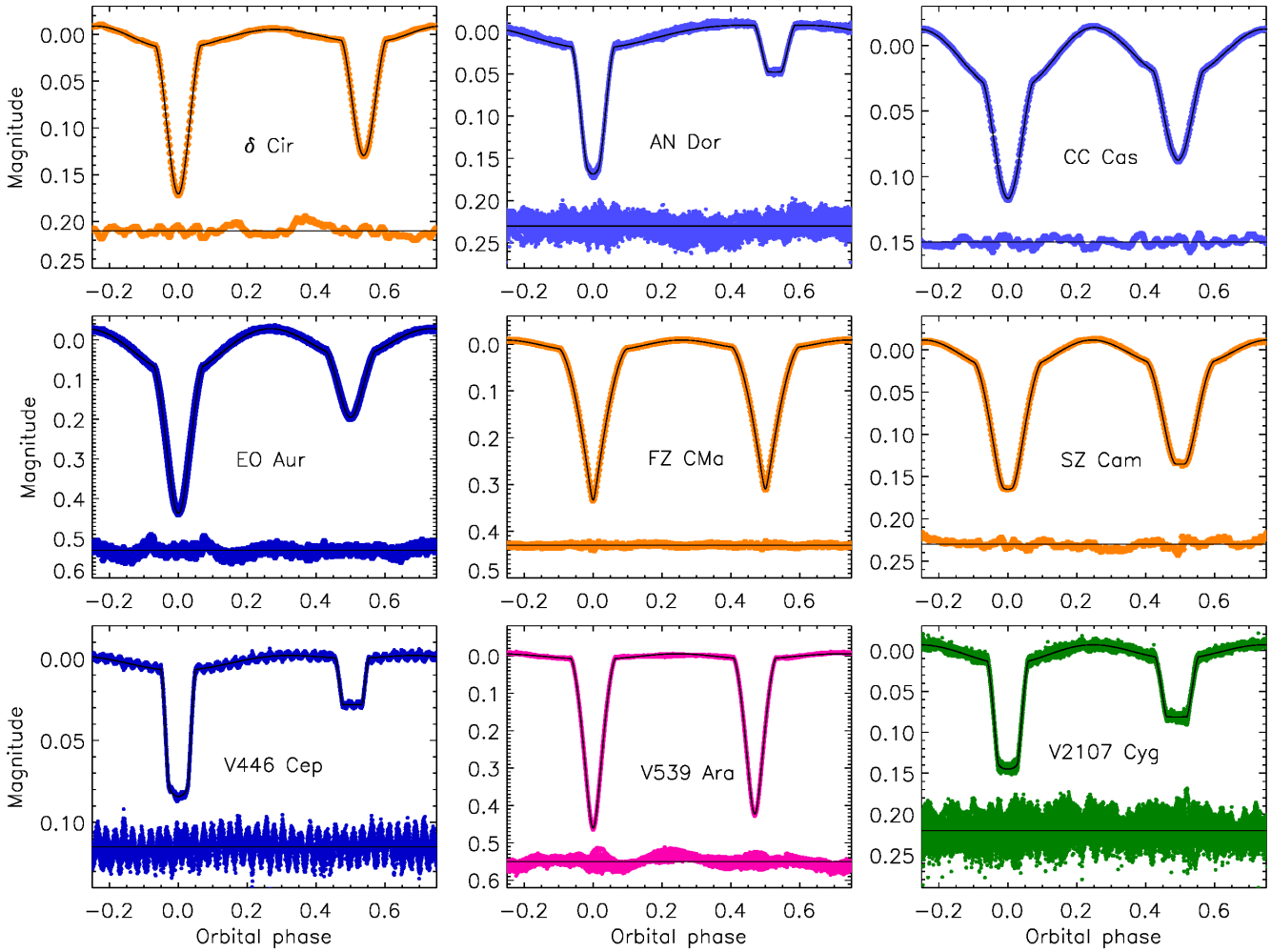

Figure 4. Fit to the TESS data for nine of the short-period systems (labelled). In each case the data are shown after subtraction of the normalisation polynomials. Those with lots of data were fitted using JKTEBOP and those with only 400 datapoints were fitted using WD2004. The best fits are shown with black lines. The residuals of the fits are shown at the base of each panel, multiplied by a factor of five to make the features easier to see. The data shown for AN Dor cover only one of the five TESS sectors, in order to decrease the size of the image file.

5.5 μ Eridani

μ Eri is another bright system with an extensive observational history, composed of an SPB star and a much smaller and less massive star in a 7.359 d orbit with an eccentricity of 0.34. It has been known to be a spectroscopic binary for over a century (Frost & Adams 1910; Frost et al. 1926; Hill 1969), and was discovered to be a pulsating variable by Handler et al. (2004) and eclipsing by Jerzykiewicz et al. (2005). Jerzykiewicz et al. (2013) presented a detailed analysis of the system based on extensive spectroscopy and 12 d of observations from the MOST satellite. They extracted pulsation frequencies, fitted the eclipses, and derived a new single-lined spectroscopic orbit.

μ Eri was observed by TESS in Sectors 5 and 32, totalling 52 d of coverage including observations of seven eclipses (Fig. 1). The pulsations strongly affect the eclipse shapes but unfortunately are not easy to remove. We therefore modelled the two sectors of data with JKTEBOP with the pulsations still present, and give only indicative parameters in Table 3. We fixed e and ω at the values given by Jerzykiewicz et al. (2013) and chose an indicative surface brightness ratio of 0.15. We expect that a more detailed analysis of these data could lead to a more robust model of the system.

Owing to the significant gap between the two available short-cadence sectors of μ Eri, we analysed the pulsational variability of both sectors independently. After manually removing the eclipses from the light curves, we did not find any significant frequencies following our S/N $\geqslant$ 5 significance criterion, despite μ Eri being a known g-mode pulsator (Handler et al. 2004; Jerzykiewicz et al. 2005, 2013). This is not surprising since in our analysis we restricted ourselves to S/N $\geqslant$ 5, whilst previous studies have pushed down to as low as S/N $\geqslant$ 3. The low-frequency g-mode regime of μ Eri, as can been seen in Fig. A1, is dense and contains multiple unresolved frequencies. These unresolved frequencies together increase the local noise level resulting in the highest amplitude peaks having S/N $<$ 5. The analysis of both pulsations and eclipses in μ Eri will greatly benefit from further spectroscopic monitoring.

5.6 AN Doradus

AN Dor shows total eclipses with the secondary (0.05 mag) much shallower than the primary (0.16 mag), plus a strong reflection ef-

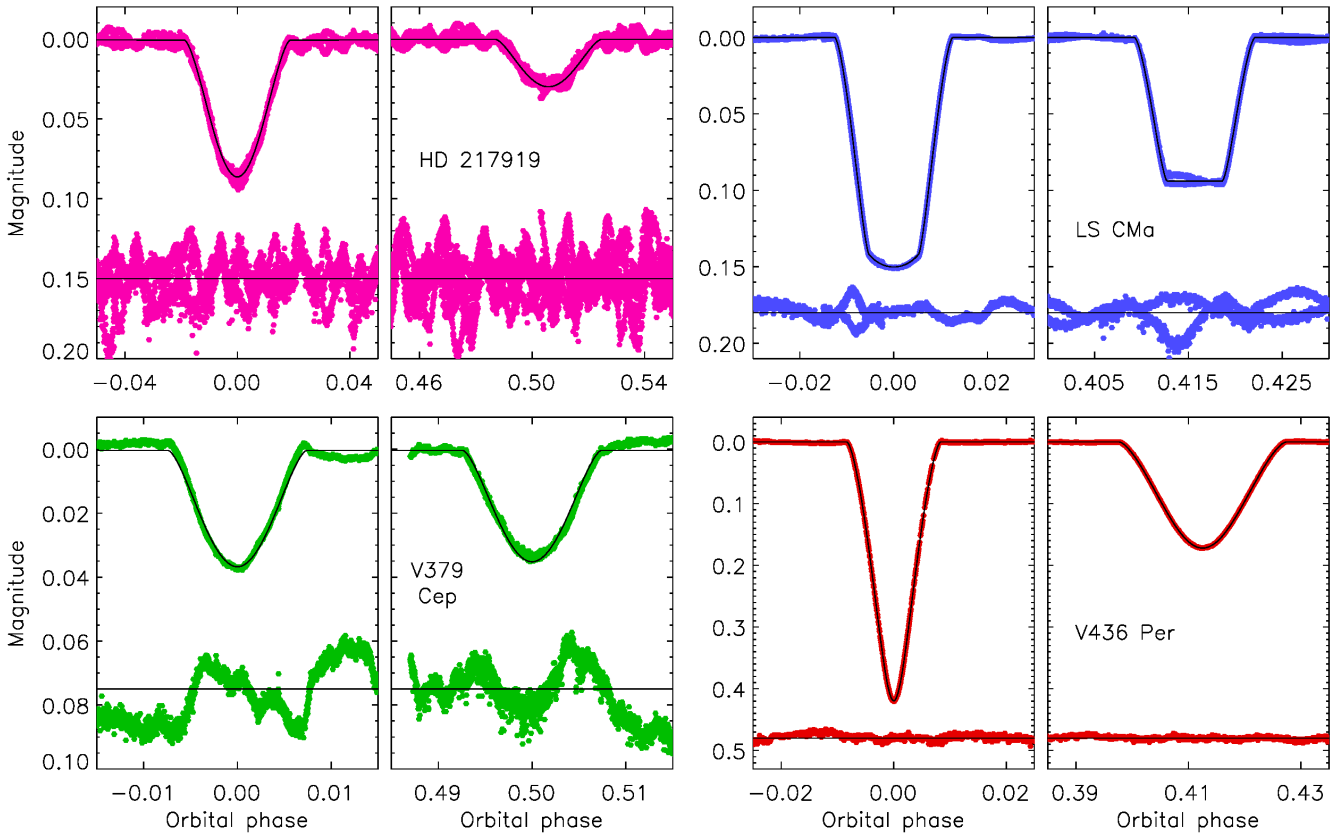

Figure 5. Fit to the TESS data for four of the long-period systems (labelled). In each case the data are shown after subtraction of the normalisation polynomials. The JKTEBOP best fits are shown with black lines. The residuals of the fit is shown at the base of each panel, multiplied by a factor of five to make the features easier to see.

fect and clear β Cephei pulsations. Little is known about this object: it was discovered to be eclipsing using *Hipparcos* satellite data and given its designation in the General Catalogue of Variable Stars by Kazarovets et al. (1999). Houk & Cowley (1975) gave its spectral type as B2/3 V. Percy & Au-Yong (2000) included it in a short list of variable B-stars in EBs, with the comment that "the short-term variability is . . . uncertain". No other study of it has been published, to our knowledge.

AN Dor has been observed extensively by TESS. It was observed in short cadence in two sets of five consecutive sectors (2–6 and 29–33), in long cadence in sectors 9, 12 and 13, and again in short cadence in sectors 36 and 39. To obtain a preliminary characterisation of the system we have analysed the light curve from sectors 29–33 (see Fig. 1) as these are sufficient for our purposes and of better quality that that from sectors 2–6. We find a good fit using JKTEBOP (Fig. 4) although star A is formally too deformed for this code to be reliable (see Table 3). Despite the short orbital period of 2.03 d the system has an eccentric orbit. Star B is smaller and much fainter than star A; the light ratio of 0.7% means extensive effort will be needed to obtain RVs for it.

For the pulsation analysis we again restricted ourselves to analysing sectors 29–33, as these data cover a long time interval and are of high quality. There are many significant frequencies in the residual amplitude spectrum of AN Dor that coincide with integer multiples of the orbital frequency. These are shown as dashed red lines in the summary figure of AN Dor in Fig. A2. We interpret the majority of these frequencies to be the result of an imperfect binary model. On the other hand, we also detect many significant independent frequencies which are indicated by green lines in Fig. A2. Given the frequency range of its variability, spanning between 1 and 16 d^{-1} with its dominant frequency range between 1 and 4 d^{-1}, and spectral type, we conclude that AN Dor is a β Cephei pulsator.

5.7 CC Cassiopeiae

CC Cas is an EB containing two close but detached stars of masses 23 $\mathrm{M}_\odot$ and 10 $\mathrm{M}_\odot$ on a 3.37 d orbit. It was discovered to be an SB2 by Pearce (1927), to be eclipsing by Guthnick & Prager (1930), and to show night-to-night variability by Polushina (1988). The most detailed study of the system was published by Hill et al. (1994), who measured the masses, radii, $T_{\rm eff}$ values and spectral types of the component stars. A more recent spectroscopic analysis by Gorda (2013) returned significantly larger masses for the two stars than in previous works, suggesting that more extensive study of this spectroscopically difficult system is needed.

CC Cas was observed by TESS in Sectors 18 and 19 (Fig. 2) and the appearance of the light curve in the two sectors is very similar. The large fractional radii of star A meant we had to perform an initial JKTEBOP analysis to obtain the orbital ephemeris, phase-bin the data, and then fit it with WD2004 (Fig. 4). The results of this work are given in Table 4. The fractional radii are measured to precisions of 1.2% and 2.5%. The orbital inclination, $65.44 \pm 0.21^\circ$, is one of the lowest known for an EB and is possible because of the large sizes of the stars relative to the orbit. It is also significantly lower than found in previous work (e.g. Hill et al. 1994 found $i =$

$69.6 \pm 0.4^\circ$) – this may have occurred due to the low quality of the photometry available before TESS or alternatively it might indicate presence of dynamical effects such as those as seen in VV Ori by Southworth et al. (2021).

The light curve solution requires a small but highly significant orbital eccentricity of $e = 0.0099 \pm 0.0013$; solutions assuming a circular orbit cannot correctly reproduce the shapes of the ingress and egress of the eclipses. Previous studies of CC Cas (e.g. Hill et al. 1994 and Gorda 2013) have assumed a circular orbit due to lack of evidence for eccentricity, but the TESS light curve is inconsistent with that assumption. We determined the physical properties of the system using our photometric analysis and the spectroscopic results from Gorda (2013), which appear to be based on the highest-quality spectra. The masses are measured to better than 4% precision and the radii to better than 2%. This system is therefore a good candidate for measuring the properties of a $23\,\mathrm{M}_\odot$ star to high precision, although extensive high-quality spectroscopy and a sophisticated analysis will be needed.

We detect no significant independent pulsation modes in the residual amplitude spectrum of CC Cas, as shown in Fig. A2. The light curve is dominated by SLF variability, which is consistent with the recent result that main-sequence O-type stars have predomimantly SLF variability rather than multiple high-amplitude heat-driven modes (Bowman et al. 2020).

5.8 EO Aurigae

EO Aur is an EB containing two early-B stars in a 4.07 d orbit. The system was discovered to be a spectroscopic binary by Pearce (1943) and to be eclipsing by Gaposchkin (1943). It has proved to be spectroscopically intractable due to the large line broadening of the components (Popper 1978; Burkholder et al. 1997) so the masses are not known with any certainty; future analysis using methods such as spectral disentangling may meet with more success (e.g. Pavlovski & Hensberge 2005; Pavlovski et al. 2018). Light curves and radius measurements have been presented by Schneller (1963) and Hartigan (1981).

EO Aur was observed in TESS Sector 19 (Fig. 2). Our JKTEBOP fit to these data is shown in Fig. 4. We get a reasonable but not a good fit, failing in particular to match the data around the times of first and fourth contact for the primary eclipse. Star A has a fractional radius too large for JKTEBOP (Table 3) and this is likely the reason for our imperfect fit. The system is in need of extensive new observations and analysis for its properties to be established reliably.

The residual amplitude spectrum of EO Aur contains four significant frequencies which coincide with integer multiples of the orbital frequency, but also a single additional independent frequency at $12.1466 \pm 0.0005\ \mathrm{d}^{-1}$. Therefore we classify EO Aur as containing a β Cephei pulsator. The summary figure of EO Aur is shown in Fig. A2. We surmise, similarly to many stars in our sample, that EO Aur is a multi-periodic β Cep pulsator, but the analysis of only a single available TESS sector does not reveal low amplitude pulsation modes.

5.9 FZ Canis Majoris

FZ CMa was discovered to show double spectral lines with variable RV by Neubauer (1943) and to be eclipsing on a 1.27 d period by Moffat & Vogt (1974). A detailed analysis of the system was presented by Moffat et al. (1983). They found excess scatter in their light curves and attributed this to intrinsic variability of the system. They also found a large third light and a light-time effect indicative of the presence of a tertiary component of large mass and an orbit with a period of 1.47 yr. The system has been spectrally classified as B2 Vn by Claria (1974), as B2.5 IV-V by Moffat & Vogt (1974), and as B2 IVn by Herbst et al. (1978). Moffat et al. (1983) obtained eight spectra which showed lines of the eclipsing stars and used these to determine preliminary masses for them. They did not spectroscopically detect the tertiary despite its large mass, which suggests it is either rotating very quickly or instead could itself be binary (Chambliss 1992). A detailed spectroscopic study of this system is needed in order to characterise it properly.

FZ CMa was observed by TESS in sectors 7 and 33, and both light curves show clear eclipses and intrinsic variability (Fig. 2). Due to the known light-time effect we modelled these separately using WD2004. The eclipses are shallow and V-shaped, and can only be fitted with a large amount of third light, as already found by Moffat et al. (1983). The amount of third light is very well determined as $\ell_3 = 0.467 \pm 0.007$, i.e. it is almost half of the total light of the system. We are able to obtain a good but not perfect fit to the TESS data (Fig. 4), and determine the fractional radii to precisions of 0.2% for the primary and 1.0% for the secondary (Table 4). To obtain our solution we adopted a $T_{\rm eff}$ for star A of 22 000 K (Moffat et al. 1983) and arbitrarily assigned an uncertainty of 2000 K to this value. The physical properties are given in Table 4 and suffer from large uncertainties in the measured velocity amplitudes. The system would benefit from a detailed spectroscopic analysis to determine precise masses and $T_{\rm eff}$ values for the component stars.

We analysed the sector 7 and 33 data for FZ CMa separately, finding that they ultimately yield similar pulsation mode frequencies. FZ CMa shows a total of four significant pulsation mode frequencies between $2 < \nu < 8\ \mathrm{d}^{-1}$ in sector 7, classifying it as a β Cephei star. The summary figures for both sectors are shown in Fig. A2.

5.10 HD 217919

HD 217919 is unique in this work as it was not previously known to be an EB, but was instead picked up by a colleague (Dr. P. Maxted) whilst browsing the TESS database. It is a known spectroscopic binary, for which Garmany (1972) presented a single-lined orbit with a period of 17.04 d and an eccentricity of 0.26; he also noted the lines appeared doubled on three of the plates. The TESS light curve shows lovely β Cephei pulsations overlaid on obvious but shallow eclipses of depth 0.09 mag (primary) and 0.03 mag (secondary).

HD 217919 has been observed by TESS in three sectors: 17, 18 and 24 (Fig. 2). The phasing of the observations is such that six secondary but only three primary eclipses were observed. The stars are well-detached so are suitable for analysis with JKTEBOP. The time interval covered by the TESS data is long enough to get a precise linear ephemeris. In Fig. 4 we show the best fit and in Table 3 we give the fitted parameters from our eclipse analysis. We find a solution with a period of 16.2 d, a small eccentricity, and a significant third light. It is therefore possible that there is a tertiary component that is responsible for the pulsations, rather than one of the eclipsing components. The presence of a bright third star will also make spectroscopic analysis of this system difficult. The solution is unstable in that separate fits of individual sectors give very different results, so we give only an indicative solution: the best fit to all data but to only a few significant figures.

We performed a frequency analysis of the two segments of

TESS data available for HD 217919 separately, although they differ somewhat in quality and the resultant frequency lists. This revealed a rather dense spectrum of significant pulsation modes that span between $1.5 < \nu < 10.5$ d^{-1}. The apparent groups of the frequencies is reminiscent of high-radial order gravity modes seens in non-linear SPB pulsators (see e.g. Kurtz et al. 2015), which can be explained at least in part by combination frequencies. However, such a phenomenum has not been seen for low-radial order p-modes in β Cephei stars, assuming that these pulsation modes are intrinsic to the primary. If they are intrinsic to the secondary or teritary, then the companions could be SPB stars. Given the frequency range and spectral types of the system, we tentatively classify these as β Cephei pulsations. They may plausibly arise in any of the three components of the system.

5.11 HQ Canis Majoris

HQ CMa was found to show variable RV by Buscombe & Morris (1960) and to be eclipsing by Jerzykiewicz & Sterken (1977). Sterken et al. (1985) presented the only known dedicated analysis of this object, establishing its orbital period as 24.6033 d. although they were not able to observe a single eclipse in its entirety.

HQ CMa has been observed by TESS in three sectors: 7, 34 and 35 (Fig. 2). Only one eclipse is visible in these data, in sector 34 and of depth 0.022 mag, but variability consistent with SPB and/or β Cephei pulsations is clearly discernable. Upon analysis with JKTEBOP we immediately discovered the period from Sterken et al. (1985) is incorrect because the data 24.6 d after the observed eclipse does not have an eclipse. A nearby gap in the data allows periods of 21.2 to 22.6 d; values of 34.5 d or longer would also be consistent with the TESS light curve. Faced with a system showing a single shallow partial eclipse and an unknown orbital period, it is a thankless task to deduce its properties so we have not attempted this. The shallowness of the eclipse can easily be matched using a grazing eclipse configuration, but it is also possible that there is a strong third light in the system in which case it is possible that the pulsations do not arise from either of the stars in the EB.

We analysed sectors 33 and 34 of the TESS data of HQ CMa in search for significant pulsations, blind to in which star they may originate. As shown in the summary figures in Fig. A1, there is evidence of both low-frequency g-modes indicative of an SPB star and high-frequency p-modes indicative of a β Cephei star. The amplitudes of the β Cephei pulsations are quite small and not all frequencies are significant in both sectors. Similarly, the presence of multiple unresolved frequencies in the low-frequency g-mode regime means that only a single g-mode frequency has S/N ≥ 5 in sector 33. Since the primary has a spectral type of B3 V, it is in the mass regime that allows for both p- and g-mode frequencies to be excited by the κ mechanism during the main sequence (Walczak et al. 2015; Szewczuk & Daszyńska-Daszkiewicz 2017). We conclude that HQ CMa contains either a candidate hybrid SPB/β Cephei pulsator, or the β Cephei pulsations originate in a contaminating source given that the secondary likely has a later spectral type that the primary, and hence is not massive enough to host β Cephei pulsations.

5.12 LS Canis Majoris

Despite its brightness, almost nothing was previously known for LS CMa. Its variability was found using the *Hipparcos* satellite and it was attributed this name and the "E:" designation in the General Catalogue of Variable Stars (Kazarovets et al. 1999). Its RV is listed as 6 km s^{-1} in the General Catalogue of Stellar Radial Velocities (Wilson 1953) and a rotational velocity of 17 km s^{-1} was given by Abt et al. (2002).

LS CMa was observed with TESS in two sets of two consecutive sectors: 6 and 7, and 33 and 34 (Fig. 2). The light curve shows clear variability aside from the eclipses. Four eclipses were observed: a secondary then part of the next primary in sectors 6 and 7, and a primary and immediately following secondary in sectors 33 and 34. The primary eclipse is annular and the secondary eclipse is total, indicating that the primary star is significantly hotter and larger than the secondary. Due to the order the eclipses were observed in, and despite the 730 d time interval between the two observed primaries (and also secondaries) it is straightforward to establish the orbital period of the system as 70 d. Using JKTEBOP we refined this and the remaining photometric parameters to the values given in Table 2. The best fit to the eclipses is shown in Fig. 5.

Frequency analysis of sectors 33 and 34 of LS CMa reveals a few significant frequencies that coincide with integer multiples of the orbital frequency. We also detect a single independent frequency in sector 33, of frequency $\nu = 1.61381 \pm 0.00006$ d^{-1} and amplitude of 0.768 ± 0.004 mmag. This frequency is not significantly detected in sector 34. LS CMa is therefore not a convincing pulsating EB system based on the data currently available. The summary figures for the frequency analysis of LS CMa are shown in Fig. A3.

5.13 SZ Camelopardalis

SZ Cam is a triple system with an inner orbital period of 2.70 d and a long observational history, having been discovered to be a spectroscopic binary by Plaskett (1924) and to be eclipsing by Guthnick & Prager (1930). Extensive investigations have been published by Wesselink (1941); Mayer et al. (2010) and Tamajo et al. (2012). There is a tertiary star that orbits the EB every approximately 55 yr. Tamajo et al. (2012) found that the third component is itself an SB1 with a period of 2.80 d, meaning that SZ Cam is a quadruple system. They also detected β Cephei pulsations in the system with a period of 0.333 d and tentatively attributed it to one of the non-eclipsing stars.

SZ Cam was observed by TESS in sector 19 (Fig. 3). We fitted these data with WD2004 assuming a circular orbit and allowing for third light (Fig. 4). The amount of third light we obtain is much greater than found by Tamajo et al. (2012), which can be explained by the large size of the apertures used to extract the light curve from the TESS data. However, many other parameters show a significant difference between our values (Table 4) and those found by Tamajo et al. (2012). This includes the orbital inclination, which might have changed due to dynamical effects, and the $T_{\rm eff}$ of star B which is inconsistent with the spectroscopic value from Tamajo et al. (2012). We deduced a value of the mass ratio from the TESS light curve: it is somewhat smaller than that obtained by Tamajo et al. (2012) from the spectroscopic orbits, and better matches values from earlier studies (see table 1 in Tamajo et al. 2012). In calculating the physical properties of the system we favoured the spectroscopic mass ratio and $T_{\rm eff}$ valus from Tamajo et al. (2012) over our own determinations. The measured radii are much less certain than the values from Tamajo et al. (2012) despite the use of the TESS data. Based on these issues, we conclude that the properties of SZ Cam are not as well es-

tablished as suggested by previous work. A new analysis of this spectroscopically-difficult system is needed.

We detect no significant independent pulsation modes in the residual amplitude spectrum of SZ Cam, as shown in Fig. A3. The light curve is dominated by SLF variability. This is not surprising given that the majority of the light contribution will be from the O9 IV primary and O-type stars are known to be dominated by SLF variability (Bowman et al. 2020). We do not detect the β Cephei pulsation mode frequency of Tamajo et al. (2012) at significant amplitude in the TESS data. This is probably because of flux dilution of the pulsating star by the O-type primary, and the high fraction of contamination from nearby stars for SZ Cam given that it is a member of a young cluster (Tamajo et al. 2012) and TESS pixels subtend a large angular size.

5.14 V379 Cephei

V379 Cep was found to exhibit variable RV by Adams et al. (1924) and to be eclipsing by Jerzykiewicz (1993); its orbital period of 99 d took some effort to establish (Clayton 1996; Gordon et al. 1998). Harmanec et al. (2007) found it to be a hierarchical quadrule system composed of two binary systems (the non-eclipsing one having a period of 158.7 d) orbiting each other every 7900 d.

V379 Cep was observed by TESS in sectors 15–17 and will be observed again in sector 55. Two eclipses are visible, one in sector 15 and one in sector 17, separated by 49.9 d (Fig. 3). Under the assumption that these are one primary and one secondary eclipse, we fitted the light curve with JKTEBOP using a fixed orbital period of 99.7658 d (Harmanec et al. 2007). Our solution (Fig. 5) is surprisingly consistent with a circular orbit, and unsurprisingly requires a large and poorly-constrained amount of third light to match the data. We adopted $\ell_3 = 0.50$ to produce an indicative solution of the TESS data, which is given in Table 3. This is lower than the value of $\ell_3 = 0.7$ adopted by Harmanec et al. (2007), but returns (slightly) more plausible system properties from the TESS light curve. Further work on this object is needed for its properties to be reliably established.

We detect no significant independent pulsation modes in the residual amplitude spectrum of V379 Cep, as shown in Fig. A3. The light curve is dominated by SLF variability.

5.15 V436 Persei

V436 Per was found to be a spectroscopic binary by Adams (1912) and to be eclipsing by Kurtz (1977). Harmanec et al. (1997) have summarised the observational history of the system, and also detected LPVs in their high-resolution spectra. These authors subsequently revisited the system (Janík et al. 2003), were unable to confirm the LPVs, and established the orbital elements to high precision using spectral disentangling.

Observations of V436 Per were obtained by TESS in sector 18 (Fig. 3), and the light curve fortuitously contains one primary and one secondary eclipse (Fig. 4). To constrain the orbital period of the system we adopted a time of minimum of HJD 2443562.861 ± 0.020 where the value comes from Janík et al. (2003) and the errorbar from Harmanec et al. (1997). The e and ω of the system are of such a value that there exists three regions in parameter space that provide a similar fit. This is illustrated in Fig. 6.

We can reject the local minimum with $k = 0.69 \pm 0.03$ on statistical grounds, as it corresponds to a significantly worse fit

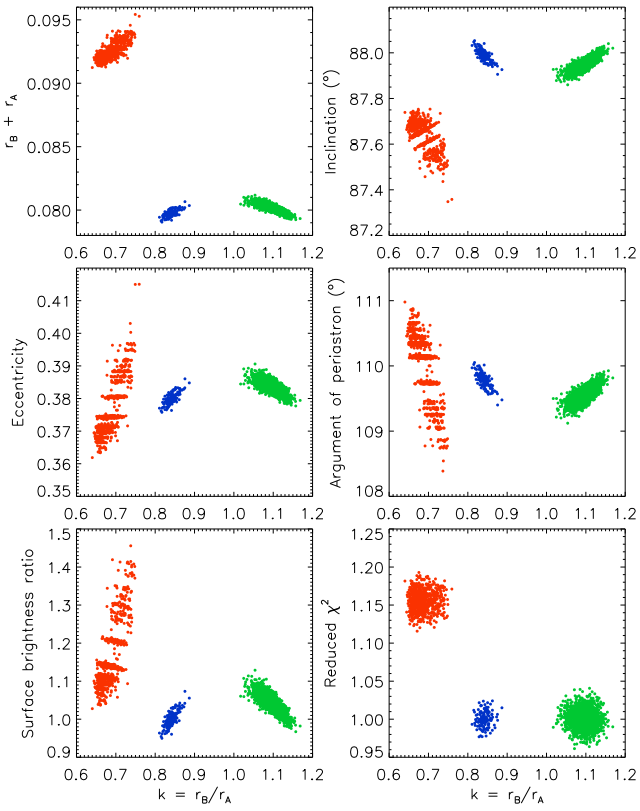

Figure 6. Monte Carlo scatter plots for V436 Per. Three local minima in parameter space are visible in the ratio of the radii. These have been represented in different colours for clarity. The preferred minimum is the one in green and is the group with the largest value of k.

(higher reduced χ^2). On closer inspection this result occurs only for unphysical values of the limb darkening coefficients. We can also reject the local minimum with $k = 0.84 \pm 0.02$ on astrophysical grounds, as it corresponds to an inverted mass–radius relationship for this binary system composed of two main-sequence stars. We therefore base our results on the third minimum ($k = 1.10 \pm 0.03$), which also is fully consistent with the e, ω and $T_{\rm eff}$ values from the extensive spectroscopic analysis of this system by Janík et al. (2003). With our results plus the velocity amplitudes from Janík et al. (2003) we establish physical properties of the system to high precision for the first time (Table 2). A confirmation of these results could come from a direct measurement of a spectroscopic light ratio, as this differs significantly between the three local minima.

We detect no significant independent pulsation modes in the residual amplitude spectrum of V436 Per, as shown in Fig. A3. The light curve is dominated by SLF variability, but additional photometry would be useful in distinguishing SLF variability from independent pulsation modes that are possibly present but insignificant in the current data.

5.16 V446 Cephei

V446 Cep was discovered to be eclipsing based on data from the *Hipparcos* satellite (Kazarovets et al. 1999), with a period of 3.81 d. Çakırlı et al. (2014) published the only dedicated analysis of the system, based on the *Hipparcos* light curve and 15 medium-resolution spectra. They assigned spectral types of B1 V and B9 V,

and determined the masses (18 and 2.6 $M_\odot$) and radii (8.3 and 2.1 $R_\odot$) of the stars.

TESS observed V446 Cep in sectors 16, 17 and 24. The light curve shows annular primary eclipses of depth 0.08 mag, total secondary eclipses of depth 0.03 mag, and multiperiodic pulsations of a few mmag amplitude (Fig. 3). Our JKTEBOP analysis required a small orbital eccentricity to fit the data properly, but no third light was needed. We were able to get a good fit to the data (Fig. 4) and evaluated the uncertainties of the resulting parameters using Monte Carlo and residual-permutation algorithms (Southworth 2008).

The surface brightness ratio of the two stars is 0.48 so their $T_{\rm eff}$ ratio should be approximately $0.48^{1/4} = 0.83$. This does not agree with the determinations by Çakırlı et al. (2014), 26600 ± 1000 K and 11900 ± 1050 K, which have a ratio of 0.45 ± 0.05. Given this discrepancy, and the preliminary nature of the published analysis, their spectroscopic results are questionable. We have therefore not determined the physical properties of the system, in favour of deferring this until more extensive spectroscopy becomes available. If the $T_{\rm eff}$ of star A from Çakırlı et al. (2014) is reliable, then our J gives a $T_{\rm eff}$ of star B of approximately 22 000 K (Table 2).

We performed a pulsation analysis of sectors 16–17 and 24 of V446 Cep separately owing to their temporal separation and difference in data quality. Most noteworthy is the presence of a high-amplitude frequency in both residual amplitude spectra which coincides with an orbital harmonic, as shown in the summary figures in Fig. A3. Specifically, 10.24372 ± 0.00006 d^{-1} with an amplitude of 1.262 ± 0.007 mmag in sectors 16–17 and 10.2437 ± 0.0002 d^{-1} with an amplitude of 1.28 ± 0.01 mmag in sector 24. There are also several independent pulsation modes spanning $2 < \nu < 12$ d^{-1}. Therefore, we conclude that V446 Cep is a candidate system for showing TEOs in addition to β Cephei pulsations. On the other hand, if the secondary is sufficiently evolved it could be a δ Scuti pulsator, but we deem this a less favourable solution given the known properties of the system.

5.17 V539 Arae

V539 Ara consists of B3 V and B4 V stars in a 3.17 d orbit. Neubauer (1930) found it to be SB2 and Strohmeier (1964) discovered eclipses. The most detailed work on this object comes from the Copenhagen group: Andersen (1983) determined a spectroscopic orbit based on extensive photographic spectroscopy, Clausen et al. (1996) presented extensive $uvby$ photometry, and Clausen (1996) measured the masses and radii of the component stars to high precision. The system shows intrinsic variability (Knipe 1971), which Clausen (1996) ascribed to SPB pulsations in the secondary star and identified three possible frequencies. V539 Ara also undergoes apsidal motion (Andersen 1983) with an apsidal period of 162 ± 8 yr. There is a tertiary companion with a period of 42.3 ± 0.8 yr (Wolf & Zejda 2005) and a wider companion at 12.3 arcsec that is fainter than the EB by approximately 3.6 mag in the *Gaia* G, BP and RP passbands.

V539 Ara was observed by TESS in sectors 13 and 39 (Fig. 3). For our JKTEBOP analysis we analysed these separately and did not consider photometry from other sources, in order to avoid issues with the apsidal motion. We allowed for an eccentric orbit and third light, and calculated uncertainties using the Monte Carlo and residual-permutation algorithms (Fig. 4). The results from the two sectors are in very good agreement so were combined according to their weighted means. The residual-permutation errorbars are larger than the Monte Carlo errorbars, which can be attributed to the variability in the light curve. Our results establish the radii of the stars to precisions of 0.4% (star A) and 1% (star B; Table 2), and are in good agreement with those from Clausen (1996).

We detect no significant independent pulsation modes in the residual amplitude spectrum of V539 Ara, as shown in Fig. A3, hence it is dominated by SLF variability. Similarly to SZ Cam, the difference in our classification of SLF variability and the SPB classification of Clausen (1996) is likely because of flux dilution of the pulsating star by the non-pulsating star, and possible contamination from the large TESS pixels. If additional light curve data become available, it is likely that the independent g-mode frequencies of Clausen (1996) would become extractable and significant.

5.18 V2107 Cygni

V2107 Cyg was observed spectroscopically by Mercier (1957), who found it to be SB1 with a small eccentricity. It was subsequently detected to be eclipsing from *Hipparcos* observations (Kazarovets et al. 1999). The only detailed study published so far is that of Bakış et al. (2014), who presented medium-resolution spectroscopy and extensive BVR photometry. They established the physical properties of the stars and detected LPVs, attributing this to β Cephei pulsations in the primary star.

V2107 Cyg has been observed by TESS in sectors 14, 15 and 41 (Fig. 3), and will also be observed in sectors 54 and 55. These show clear β Cephei pulsations superimposed on total and annular eclipses. Our JKTEBOP fit (Fig. 4) included an eccentric orbit but not third light, as this is not well determined by the data. The primary star is tidally deformed beyond the limits of applicability of JKTEBOP, and the velocity amplitude of the secondary star is uncertain (Bakış et al. 2014) so we give only approximate values for the properties of the components (Table 3).

Our frequency analysis of the residual light curve of V2107 Cyg reveals a multiperiodic pulsator with a frequency range spanning $0.37 < \nu < 9.21$ d^{-1}. Combined with the spectral type of B1 III, this confirms the pulsator class identification of β Cephei. We find no regular structure or patterns in the frequency spectrum of observed pulsations indicative of rotational splittings or tidally perturbed modes, which is interesting given its significantly distorted structure (see e.g. Southworth et al. 2020, 2021). We conclude that the V2107 Cyg is a valuable system for follow-up study. We are in the process of obtaining new high-quality spectroscopy and will perform a detailed analysis of the system in due course.

6 SUMMARY AND DISCUSSION

We present the analysis of TESS data for 18 eclipsing binary systems containing pulsating high-mass stars. Of these, eleven are definite or candidate β Cephei pulsators, six are SPB pulsations and eight have light curves and amplitude spectra dominated by SLF variability. Most of the pulsation detections are new, and significantly increase the number of EBs known to contain stars with these types of pulsations. We fitted the light curves with two EB models to determine the properties of the systems and remove the effects of binarity from the TESS data. These residual light curves were then subjected to frequency analysis to classify the pulsations and measure pulsation frequencies and amplitudes. Future work, guided by additional spectroscopy and TESS photometry, will aid in indentifying the geometries of the identified pulsation mode frequencies, which is typically a prerequisite for forward asteroseismic modelling.

Spectroscopic orbits are available in the literature for several of these EBs, and in these cases the full physical properties of the system were calculated based on the literature spectroscopy and the TESS data. We determined precise physical properties for five systems (δ Cir, CC Cas, SZ Cam V436 Per and V539 Ara) and preliminary physical properties for four more. Many of the objects studied in this work show lovely eclipses and pulsations and are promising candidates for detailed study. We have already begun a spectroscopic survey of the best candidates and will present results in due course.

The study of pulsating high-mass stars in EBs is an important new avenue for constraining the physics of these objects. In particular, the amount and shape of the interior mixing profiles of massive stars are unconstrained and there is ever-growing evidence that current stellar structure models underpredict the mixing in massive EBs (Tkachenko et al. 2020). When coupled with asteroseismology, the conclusion of needing extra mixing is strengthened further (Johnston 2021).

Another important constraint that pulsations within massive binaries can provide are on the impact of tides on stellar structure. In the case of short-period, near-circular binaries, the effect of tides can modify the equilibrium structure such that this is detected in the pulsation frequency spectrum (Southworth et al. 2020, 2021). There are few such detections of so-called tidally-perturbed pulsation modes in massive binaries. Therefore, a larger survey of constraining the impact of tides on binary star evolution theory probed by pulsations is needed.

Finally, an important constraint that pulsating massive binaries may provide is on the excitation mechanism(s) of pulsation modes. It is known that the heat-engine mechanism is strongly dependent on the opacity and rotation of a star (e.g. Szewczuk & Daszyńska-Daszkiewicz 2017). However, it is often difficult to determine an accurate mass and age of a massive star from spectroscopy or evolutionary models alone. The dynamical masses of EBs provide model-independent masses that can be used to more accurately constrain the parameter space of pulsations in the HR diagram. Thus the impact of binary interaction and the excitation physics of pulsations among early-type stars is now possible to study thanks to high-precision TESS data for a large sample of massive stars.

DATA AVAILABILITY

All data underlying this article are available in the MAST archive (https://mast.stsci.edu/portal/Mashup/Clients/Mast/Portal.html).

ACKNOWLEDGEMENTS

We thank Pierre Maxted for alerting us to HD 217919. The TESS data presented in this paper were obtained from the Mikulski Archive for Space Telescopes (MAST) at the Space Telescope Science Institute (STScI). STScI is operated by the Association of Universities for Research in Astronomy, Inc., under NASA contract NAS5-26555. Support to MAST for these data is provided by the NASA Office of Space Science via grant NAG5-7584 and by other grants and contracts. Funding for the TESS mission is provided by the NASA Explorer Program. This research has made use of the SIMBAD database, operated at CDS, Strasbourg, France; the SAO/NASA Astrophysics Data System; and the VizieR catalogue access tool, CDS, Strasbourg, France. DMB gratefully acknowledges funding from the Research Foundation Flanders (FWO) by means of a senior postdoctoral fellowship with grant agreement no. 1286521N.

REFERENCES

Abt H. A., Levato H., Grosso M., 2002, ApJ, 573, 359
Adams W. S., 1912, ApJ, 35, 163
Adams W. S., Joy A. H., Sanford R. F., 1924, PASP, 36, 137
Aerts C., 2021, Reviews of Modern Physics, 93, 015001
Aerts C., Lehmann H., Briquet M., Scuflaire R., Dupret M. A., De Ridder J., Thoul A., 2003, A&A, 399, 639
Aerts C., Puls J., Godart M., Dupret M. A., 2009, A&A, 508, 409
Aerts C., Christensen-Dalsgaard J., Kurtz D. W., 2010, Asteroseismology. Astron. and Astroph. Library, Springer Netherlands, Amsterdam
Andersen J., 1983, A&A, 118, 255
Andersen J., Clausen J. V., Nordström B., 1990, ApJ, 363, L33
Bakış V., et al., 2014, AJ, 147, 149
Balega I. I., Balega Y. Y., Hofmann K. H., Tokovinin A. A., Weigelt G. P., 1999, Astronomy Letters, 25, 797
Baran A. S., Koen C., 2021, AcA, 71, 113
Beardsley W. R., Zizka E. R., 1980, in BAAS. p. 452
Belczynski K., et al., 2020, A&A, 636, A104
Berghöfer T. W., Vennes S., Dupuis J., 2000, ApJ, 538, 854
Bowman D. M., 2020, Frontiers in Astronomy and Space Sciences, 7, 70
Bowman D. M., Michielsen M., 2021, A&A, in press, arXiv:2109.10776
Bowman D. M., et al., 2019a, Nature Astronomy, 3, 760
Bowman D. M., et al., 2019b, A&A, 621, A135
Bowman D. M., Burssens S., Simón-Díaz S., Edelmann P. V. F., Rogers T. M., Horst L., Röpke F. K., Aerts C., 2020, A&A, 640, A36
Bowman D. M., et al., 2021, A&A, in press, arXiv:2111.09814
Breger M., et al., 1993, A&A, 271, 482
Bruntt H., Southworth J., 2008, in Journal of Physics Conference Series. p. 012012
Budding E., Love T., Blackford M. G., Banks T., Rhodes M. J., 2021, MNRAS, 502, 6032
Burkholder V., Massey P., Morrell N., 1997, ApJ, 490, 328
Burssens S., et al., 2020, A&A, 639, A81
Buscombe W., Morris P. M., 1960, MNRAS, 121, 263
Cantiello M., Lecoanet D., Jermyn A. S., Grassitelli L., 2021, ApJ, 915, 112
Chambliss C. R., 1992, PASP, 104, 663
Chrimes A. A., Stanway E. R., Eldridge J. J., 2020, MNRAS, 491, 3479
Claret A., 1998, A&AS, 131, 395
Claret A., 2017, A&A, 600, A30
Claria J. J., 1974, AJ, 79, 1022
Clausen J. V., 1996, A&A, 308, 151
Clausen J. V., Garcia J. M., Gimenez A., Helt B. E., Jensen K. S., Suso J., Vaz L. P. R., 1996, A&AS, 115, 315
Clayton G. C., 1996, PASP, 108, 401
De Mey K., Aerts C., Waelkens C., Van Winckel H., 1996, A&A, 310, 164
De Mey K., Aerts C., Waelkens C., Cranmer S. R., Schrijvers C., Telting J. H., Daems K., Meeus G., 1997, A&A, 324, 1096
Dziembowski W. A., Pamyatnykh A. A., 1993, MNRAS, 262, 204
Dziembowski W. A., Moskalik P., Pamyatnykh A. A., 1993, MNRAS, 265, 588
Edelmann P. V. F., Ratnasingam R. P., Pedersen M. G., Bowman D. M., Prat V., Rogers T. M., 2019, ApJ, 876, 4
Frost E. B., Adams W. S., 1910, Sci, 32, 876
Frost E. B., Barrett S. B., Struve O., 1926, ApJ, 64, 1
Gaposchkin S., 1943, PASP, 55, 192
Garmany C. D., 1972, AJ, 77, 38
Gorda S. Y., 2013, Astrophysical Bulletin, 68, 101
Gordon K. D., Clayton G. C., Smith T. L., Aufdenberg J. P., Drilling J. S., Hanson M. M., Anderson C. M., Mulliss C. L., 1998, AJ, 115, 2561

Grassitelli L., Fossati L., Simón-Diáz S., Langer N., Castro N., Sanyal D., 2015, ApJ, 808, L31
Grassitelli L., Fossati L., Langer N., Simón-Díaz S., Castro N., Sanyal D., 2016, A&A, 593, A14
Guthnick P., Prager R., 1930, Astronomische Nachrichten, 239, 13
Handler G., Schwarzenberg-Czerny A., 2013, A&A, 557, A1
Handler G., et al., 2004, MNRAS, 347, 454
Harmanec P., Hadrava P., Yang S., Holmgren D., North P., Koubsky P., Kubat J., Poretti E., 1997, A&A, 319, 867
Harmanec P., et al., 2007, A&A, 463, 1061
Hartigan P., 1981, JAAVSO, 10, 13
Herbst W., Racine R., Warner J. W., 1978, ApJ, 223, 471
Hilditch R. W., 2001, An Introduction to Close Binary Stars. Cambridge University Press, Cambridge, UK
Hill G., 1969, Publications of the Dominion Astrophysical Observatory Victoria, 13, 323
Hill G., Hilditch R. W., Aikman G. C. L., Khalesseh B., 1994, A&A, 282, 455
Horst L., Edelmann P. V. F., Andrássy R., Röpke F. K., Bowman D. M., Aerts C., Ratnasingam R. P., 2020, A&A, 641, A18
Houk N., Cowley A. P., 1975, University of Michigan Catalogue of two-dimensional spectral types for the HD stars. Volume I. Declinations -90 to -53 degrees
IJspeert L. W., Tkachenko A., Johnston C., Garcia S., De Ridder J., Van Reeth T., Aerts C., 2021, A&A, 652, A120
Janík J., et al., 2003, A&A, 408, 611
Jenkins J. M., et al., 2016, in Proc. SPIE. p. 99133E
Jerzykiewicz M., 1980, Lecture Notes in Physics, 125, 125
Jerzykiewicz M., 1993, A&AS, 97, 421
Jerzykiewicz M., Sterken C., 1977, AcA, 27, 365
Jerzykiewicz M., Handler G., Shobbrook R. R., Pigulski A., Medupe R., Mokgwetsi T., Tlhagwane P., Rodríguez E., 2005, MNRAS, 360, 619
Jerzykiewicz M., et al., 2013, MNRAS, 432, 1032
Jerzykiewicz M., et al., 2015, MNRAS, 454, 724
Johnston C., 2021, A&A, 655, A29
Johnston C., Tkachenko A., Aerts C., Molenberghs G., Bowman D. M., Pedersen M. G., Buysschaert B., Pápics P. I., 2019, MNRAS, 482, 1231
Kazarovets E. V., Samus N. N., Durlevich O. V., Frolov M. S., Antipin S. V., Kireeva N. N., Pastukhova E. N., 1999, Information Bulletin on Variable Stars, 4659, 1
Knipe G. F. G., 1971, A&A, 14, 70
Kobulnicky H. A., et al., 2014, ApJS, 213, 34
Koch R. H., Hrivnak B. J., Bradstreet D. H., 1980, 12, 452
Kopal Z., 1950, Harvard College Observatory Circular, 454, 1
Kunz J., Stebbins J., 1916, in Publications of the American Astronomical Society. p. 272
Kurtz D. W., 1977, PASP, 89, 939
Kurtz D. W., 1985, MNRAS, 213, 773
Kurtz D. W., Shibahashi H., Murphy S. J., Bedding T. R., Bowman D. M., 2015, MNRAS, 450, 3015
Labadie-Bartz J., et al., 2020, AJ, 160, 32
Lee O. J., 1910, ApJ, 32, 300
Lee J. W., Hong K., 2021, AJ, 161, 32
Lee W. B., Sung E. C., Koch R. H., Hrivnak B. J., Bradstreet D. H., Corcoran M., Mitchell R. J., Blitzstein W., 1993, in Leung K.-C., Nha I.-S., eds, Astronomical Society of the Pacific Conference Series Vol. 38, New Frontiers in Binary Star Research. p. 239
Lehmann H., et al., 2001, A&A, 367, 236
Maíz Apellániz J., Barbá R. H., Simón-Díaz S., Sota A., Trigueros Páez E., Caballero J. A., Alfaro E. J., 2018, A&A, 615, A161
Mason B. D., Wycoff G. L., Hartkopf W. I., Douglass G. G., Worley C. E., 2001, AJ, 122, 3466
Maxted P. F. L., et al., 2020, MNRAS, 498, 332
Mayer P., Drechsel H., Kubát J., Šlechta M., 2010, A&A, 524, A1
Mayer P., Harmanec P., Sana H., Le Bouquin J.-B., 2014, AJ, 148, 114
Mercier J. P., 1957, Journal des Observateurs, 40, 12
Moffat A. F. J., Vogt N., 1974, A&A, 30, 381
Moffat A. F. J., Vogt N., Vaz L. P. R., Gronbech B., 1983, A&A, 120, 278
Neubauer F. J., 1930, Lick Observatory Bulletin, 429, 46
Neubauer F. J., 1943, ApJ, 97, 300
Nieva M. F., Przybilla N., 2012, A&A, 539, A143
Pavlovski K., Hensberge H., 2005, A&A, 439, 309
Pavlovski K., Southworth J., Tamajo E., 2018, MNRAS, 481, 3129
Pearce J. A., 1927, Publications of the Dominion Astrophysical Observatory Victoria, 4, 67
Pearce J. A., 1943, PAAS, 10, 322
Penny L. R., Seyle D., Gies D. R., Harvin J. A., Bagnuolo William G. J., Thaller M. L., Fullerton A. W., Kaper L., 2001, ApJ, 548, 889
Pepper J., et al., 2007, PASP, 119, 923
Percy J. R., Au-Yong K., 2000, IBVS, 4825, 1
Plaskett J. S., 1924, Publications of the Dominion Astrophysical Observatory Victoria, 2, 287
Podsiadlowski P., Rappaport S., Pfahl E. D., 2002, ApJ, 565, 1107
Podsiadlowski P., Mazzali P. A., Nomoto K., Lazzati D., Cappellaro E., 2004, ApJ, 607, L17
Polushina T. S., 1988, Peremennye Zvezdy, 22, 834
Popper D. M., 1978, ApJ, 220, L11
Prša A., et al., 2016, AJ, 152, 41
Prša A., et al., 2021, ApJS, in press, arXiv:2110.13382
Ribas I., Jordi C., Giménez Á., 2000, MNRAS, 318, L55
Ricker G. R., et al., 2015, Journal of Astronomical Telescopes, Instruments, and Systems, 1, 014003
Rogers T. M., McElwaine J. N., 2017, ApJ, 848, L1
Rogers T. M., Lin D. N. C., McElwaine J. N., Lau H. H. B., 2013, ApJ, 772, 21
Sana H., et al., 2012, Science, 337, 444
Sana H., et al., 2014, ApJS, 215, 15
Schmid V. S., Aerts C., 2016, A&A, 592, A116
Schneller H., 1963, AN, 287, 49
Schultz W. C., Bildsten L., Jiang Y.-F., 2021, ApJ Letters, submitted, arXiv:2110.13944
Simón-Díaz S., Herrero A., Uytterhoeven K., Castro N., Aerts C., Puls J., 2010, ApJ, 720, L174
Simón-Díaz S., Godart M., Castro N., Herrero A., Aerts C., Puls J., Telting J., Grassitelli L., 2017, A&A, 597, A22
Southworth J., 2008, MNRAS, 386, 1644
Southworth J., 2013, A&A, 557, A119
Southworth J., 2020, The Observatory, 140, 247
Southworth J., 2021, Universe, 7, 369
Southworth J., Maxted P. F. L., Smalley B., 2004, MNRAS, 351, 1277
Southworth J., Maxted P. F. L., Smalley B., 2005, A&A, 429, 645
Southworth J., Wheatley P. J., Sams G., 2007a, MNRAS, 379, L11
Southworth J., Bruntt H., Buzasi D. L., 2007b, A&A, 467, 1215
Southworth J., et al., 2011, MNRAS, 414, 2413
Southworth J., Bowman D., Tkachenko A., Pavlovski K., 2020, MNRAS, 497, L19
Southworth J., Bowman D. M., Pavlovski K., 2021, MNRAS, 501, L65
Stankov A., Handler G., 2005, ApJS, 158, 193
Sterken C., Duerbeck H. W., Hensberge H., Manfroid J., Stahl O., Linden D. V., 1985, A&AS, 60, 1
Stickland D. J., Koch R. H., Pachoulakis I., Pfeiffer R. J., 1993, The Observatory, 113, 139
Strohmeier W., 1964, IBVS, 49, 2
Szewczuk W., Daszyńska-Daszkiewicz J., 2017, MNRAS, 469, 13
Tamajo E., Munari U., Siviero A., Tomasella L., Dallaporta S., 2012, A&A, 539, A139
Tango W. J., et al., 2006, MNRAS, 370, 884
Thompson S. E., et al., 2012, ApJ, 753, 86
Tkachenko A., et al., 2012, MNRAS, 424, L21
Tkachenko A., et al., 2014, MNRAS, 438, 3093
Tkachenko A., et al., 2020, A&A, 637, A60
Torres G., Andersen J., Giménez A., 2010, A&ARv, 18, 67
Uytterhoeven K., Willems B., Lefever K., Aerts C., Telting J. H., Kolb U., 2004a, A&A, 427, 581
Uytterhoeven K., Telting J. H., Aerts C., Willems B., 2004b, A&A, 427, 593

Van Hamme W., 1993, AJ, 106, 2096
Waelkens C., 1991, A&A, 246, 453
Waelkens C., Lampens P., 1988, A&A, 194, 143
Walczak P., Fontes C. J., Colgan J., Kilcrease D. P., Guzik J. A., 2015, A&A, 580, L9
Walker M. F., 1951, PASP, 63, 35
Welsh W. F., et al., 2011, ApJS, 197, 4
Wesselink A. J., 1941, Annalen van de Sterrewacht te Leiden, 17, C1
Wilson R. E., 1953, Carnegie Institute Washington D.C. Publication, p. 0
Wilson R. E., 1979, ApJ, 234, 1054
Wilson R. E., Devinney E. J., 1971, ApJ, 166, 605
Wilson R. E., Van Hamme W., 2004, Computing Binary Star Observables (Wilson-Devinney program user guide), available at ftp://ftp.astro.ufl.edu/pub/wilson
Wolf M., Zejda M., 2005, A&A, 437, 545
Çakırlı Ö., Ibanoglu C., Sipahi E., Frasca A., Catanzaro G., 2014, New Astronomy, submitted, arXiv:1406.0499

This paper has been typeset from a TEX/LATEX file prepared by the author.